Article

Fault Detection of Wind Turbine Induction Generators through Current Signals and Various Signal Processing Techniques

Yuri Merizalde [1,*] , **Luis Hernández-Callejo** [2,*] , **Oscar Duque-Perez** [3]
and Raúl Alberto López-Meraz [4]

1 PhD School of the University of Valladolid (UVA), Faculty of Chemical Engineering,
   University of Guayaquil, Clemente Ballen and Ismael Perez Pazmiño, Guayaquil 593, Ecuador
2 Department of Agricultural Engineering and Forestry, University of Valladolid (UVA),
   Campus Universitario, Duques de Soria, 42004 Soria, Spain
3 Department of Electrical Engineering, University of Valladolid (UVA), Escuela de Ingenierías Industriales,
   Paseo del Cauce 59, 47011 Valladolid, Spain; oscar.duque@eii.uva.es
4 Unidad de Ingeniería y Ciencias Químicas, Universidad Verzcruzana, Circuito Universitario Gonzalo
   Aguirre Beltrán, Zona Universitaria, Xalapa 91000, Mexico; meraz_raul@hotmail.com
* Correspondence: yuri.merizaldez@ug.edu.ec (Y.M.); luis.hernandez.callejo@uva.es (L.H.-C.);
   Tel.: +34-975-129-418 (L.H.-C.)

check for
updates

Abstract: In the wind industry (WI), a robust and effective maintenance system is essential. To minimize the maintenance cost, a large number of methodologies and mathematical models for predictive maintenance have been developed. Fault detection and diagnosis are carried out by processing and analyzing various types of signals, with the vibration signal predominating. In addition, most of the published proposals for wind turbine (WT) fault detection and diagnosis have used simulations and test benches. Based on previous work, this research report focuses on fault diagnosis, in this case using the electrical signal from an operating WT electric generator and applying various signal analysis and processing techniques to compare the effectiveness of each. The WT used for this research is 20 years old and works with a squirrel-cage induction generator (SCIG) which, according to the wind farm control systems, was fault-free. As a result, it has been possible to verify the feasibility of using the current signal to detect and diagnose faults through spectral analysis (SA) using a fast Fourier transform (FFT), periodogram, spectrogram, and scalogram.

Keywords: wind turbine; electric generator; spectral analysis; fault diagnosis

1. Introduction

Regardless of the maintenance strategies and models applied in the wind industry (WI) to detect and diagnose faults, the use of signals, such as vibration, acoustic, temperature, magnetism, and electrical signals, is an indispensable requirement. Each of these types of signal have their advantages and disadvantages. However, because all moving equipment produces some type of vibration, in the WI, the use of vibration signals predominates [1–3]. Even though the current signal does not use intrusive methods, the equipment used is inexpensive, easy to install, and also, according to reference [4,5], both the vibration and current signal can be used to detect failures of the electric generator and loads coupled to its axis. However, according to published reports, in the WI, current signals have rarely been used, and the existing research is based predominantly on laboratory studies.

The processing of the signals used for the detection and diagnosis of faults is carried out using a variety of models in the time, frequency, and time–frequency domains. All signal processing techniques

have their own advantages and disadvantages, and the same applies to the domain in which the analysis is carried out [1–4]. Furthermore, the lack of ideal conditions to apply a specific technique directly prompts us to develop mathematical models that allow the detection and diagnosis of a specific type of fault that occurs in a particular component and in certain specific conditions of operation [6–8]. The combination of all these factors has given rise to a huge number of proposed methods, some of which are analyzed in more detail in the following sections.

Based on the foregoing, the purpose of this research is the detection and diagnosis of electrical generator faults by means of the current signal of real wind turbines (WTs) in operation and the application of various techniques for processing and analyzing existing signals to:

- Analyze the models used to detect the frequency components associated with faults.
- Obtain the spectrum of the current signal of an operating turbine.
- Study the effectiveness of signal processing techniques in detecting WT failures.
- Check the effectiveness of the WT control system to determine the status of the generator.
- Compare the results obtained with those of previously published studies.

Due to the variety of stresses to which the rotary induction machine is subjected, there are a variety of failures that can occur in the stator, rotor, and bearings, as described in reference [9]. The objective of this research is not to focus on a specific fault, but rather, applying the different signal processing techniques, try to detect and diagnose the faults that will be described in sections two and three. As one of the main objectives of this research is to use data from WTs in operation, and the only wind farm (WF) available to make the measurements was integrated by WTs that use SCIG, then the study will focus on this type of electric generator. The remainder of this original research is organized as follows. Section 2 analyzes the mathematical models used to determine the frequency components associated with faults in the SCIG using current signal analysis. In Section 3, the fundamentals and application of various signal analysis techniques are discussed, emphasizing the published techniques for fault detection in WTs using the SCIG current signal. Section 4 details the methodology and materials used for the experimental part of this research. Section 5 includes the results obtained by applying the techniques described in Section 3. Finally, the conclusions and recommendations are included in Section 6.

2. Modeling Electrical Generator Faults Using the Current Signal

Due to its design, durability, and low cost, the use of the squirrel-cage induction machine predominates at the industrial, commercial, and domestic levels [10,11]. Although there are several types of generators, according to reference [12], in the WI, the doubly fed induction generator (DFIG), and the squirrel-cage induction generator (SCIG) predominate.

The voltage signals, current, magnetic field, magnetomotive force (MMF), torque, and power of an induction machine are characterized by its sinusoidal behavior [13]. Since the speed of the rotor depends on the coefficients of the associated differential equations, which vary with time, the behavior of the materials used in the construction of the motor is not constant over time but depends on the position of the rotor. Under these conditions, it is hard to analyze signals in a spatial system, which is why in-plane analysis is preferred. For this purpose, using the Clarke and Park transforms, a change of variables is made. With the first transformation, we go from a 3D system (abc) to a 2D plane (alpha-beta) that varies with the stator, while with the second one, we obtain a plane dq0 equivalent to a 2D plane that rotates at the same rotor speed but is offset by an angle θ. Since the three-phase induction machine generally does not use a neutral line, the main current does not have a homopolar component, and the three phases can be represented in the dq plane. In this plane, the stator remains fixed (direct axis d) in relation to a rotor plane (quadrature axis q) that rotates at speed ω_x [13–15].

The transformation between the abc space system and the dq0 plane, when the latter is oriented at an angle θ with reference to the axis that remains fixed, can be performed directly using Equations (1) and (2). When θ is zero, these Equations become (3) and (4), respectively [15–18].

$$
\begin{bmatrix} i_{qs} \\ i_{ds} \\ i_{0s} \end{bmatrix} = \frac{2}{3} \begin{bmatrix} \cos\theta & \cos(\theta - \frac{2\pi}{3}) & \cos(\theta + \frac{2\pi}{3}) \\ \sin\theta & \sin(\theta - \frac{2\pi}{3}) & \sin(\theta + \frac{2\pi}{3}) \\ 0.5 & 0.5 & 0.5 \end{bmatrix} \begin{bmatrix} i_a \\ i_b \\ i_c \end{bmatrix}
\tag{1}
$$

$$
\begin{bmatrix} i_a \\ i_b \\ i_c \end{bmatrix} = \begin{bmatrix} \cos\theta & \sin\theta & 1 \\ \cos(\theta - \frac{2\pi}{3}) & \sin(\theta - \frac{2\pi}{3}) & 1 \\ \cos(\theta + \frac{2\pi}{3}) & \sin(\theta + \frac{2\pi}{3}) & 1 \end{bmatrix} \begin{bmatrix} i_{qs} \\ i_{ds} \\ i_{0s} \end{bmatrix}
\tag{2}
$$

$$
\begin{bmatrix} i_{qs} \\ i_{ds} \end{bmatrix} = \frac{2}{3} \begin{bmatrix} 1 & -\frac{1}{2} & -\frac{1}{2} \\ 0 & \frac{\sqrt{3}}{2} & -\frac{\sqrt{3}}{2} \end{bmatrix} \begin{bmatrix} i_a \\ i_b \\ i_c \end{bmatrix}
\tag{3}
$$

$$
\begin{bmatrix} i_a \\ i_b \\ i_c \end{bmatrix} = \begin{bmatrix} 1 & 0 \\ -\frac{1}{2} & -\frac{\sqrt{3}}{2} \\ -\frac{1}{2} & \frac{\sqrt{3}}{2} \end{bmatrix} \begin{bmatrix} i_{qs} \\ i_{ds} \end{bmatrix}
\tag{4}
$$

According to reference [16], the phase current of the DFIG can be expressed as a function of the flow and torque vectors (the torque angle is 90° over the flow), Equations (5) and (6), respectively, which can be represented in the dq plane, according to Equation (2). Since the variables of Equations (5) and (6) rotate at speed 2πfs, they cannot be measured directly, so it is necessary to apply the inverse Park transform to obtain the phase currents according to Equations (7) to (9). As described previously [19], the different stresses that cause a torque on the rotor include coupled loads; unbalanced dynamic forces; torsional vibration; transient torques; magnetic forces caused by leakage flux over the slots, making them vibrate at twice the frequency of the rotor; air gap eccentricity; centrifugal forces; thermal stresses caused by heat in the short-circuit ring and heat in the bars during starting (skin effect); residual forces due to casting; machining and welding. Under normal operating conditions, the spectrum of the signal has defined components. However, the asymmetries of the generator and the loads coupled to it (gearbox, blades) transmit torsional vibrations that act on the rotor, causing variations in the speed, torque, air gap magnetic flux and current bars. In this way, both mechanical and electrical faults manifest as lateral components of the fundamental wave. The number of harmonics and their amplitude depend on the magnitude of the fault [20,21].

$$
i_{sM} = i_{sM_0} + \sum A_{sM_i} sin(2\pi f_v t + \varphi_{M_i})
\tag{5}
$$

$$
i_{sT} = i_{sT_0} + \sum A_{sT_i} cos(2\pi f_v t + \varphi_{T_i})
\tag{6}
$$

$$
\begin{aligned}
i_a(t) &= i_0 \sin(2\pi f_s t + \varphi_0) \\
&+ \tfrac{1}{2}\{A_{sMi} \cos[2\pi(f_s - f_v)t - \varphi_M] \\
&+ A_{sT_i} \cos[2\pi(f_s - f_v)t - \varphi_T]\} \\
&- \tfrac{1}{2}\{A_{sM_i} \cos[2\pi(f_s + f_v)t + \varphi_M] \\
&- A_{sT_i} \cos[2\pi(f_s + f_v)t + \varphi_T]\}
\end{aligned}
\tag{7}
$$

$$
i_0 = \sqrt{i_{sM0}^2 + i_{sT0}^2}
\tag{8}
$$

$$
\varphi_0 = tg^{-1} \frac{i_{sT0}}{i_{sM0}}
\tag{9}
$$

As described in reference [22], in a fault-free machine, the rotor and stator currents should be balanced. However, due to small differences in the winding geometry and the nonlinearity of the

materials, an asymmetry arises that causes axial flow dispersion. Under these conditions, the distribution of the harmonics in the air gap undergo alterations that can be easily detected, so that we can detect broken rotor bars, one-phase failure, dynamic eccentricity, a negative sequence phase, and short circuits in the rotor and stator windings. According to the same author, in a three-phase machine, with a full pole-pass and fed by a balanced frequency ω_s, the spatial distribution of the harmonics of the MMF about the stator and as a function of the air gap flux is given by Equation (10). To apply these Equations to the rotor, θ is given by (11) or (12). Substituting these Equations in the general term of (10) and expanding it to obtain the first terms, we obtain Equation (13), which provides the components of the frequency spectrum of the current induced in the rotor by the harmonics of the air gap. That is, the stator current spectrum (CS) includes the components of the supply current and those of the rotor. The presence of short circuits between turns produces an MMF with its own frequency spectrum that is superimposed on the main one to give rise to a new spectrum that is expressed by (14) and whose main term is (15).

$$\begin{aligned} \Phi_s = \Phi_1 \cos\left(\omega t - p\theta_s\right) + \Phi_5 \cos\left(\omega t + 5p\theta_s\right) \\ -\Phi_7 \cos\left(\omega t - 7p\theta_s\right) + \Phi_{11} \cos\left(\omega t + 11p\theta_s\right) \ldots \ldots \Phi_n \cos\left(\omega t + np\theta_s\right) \end{aligned} \tag{10}$$

$$\theta = \theta_r + \theta_{sr} = \theta\_r + \omega_r t \tag{11}$$

$$\omega_r = \omega(1-s)/p \tag{12}$$

$$\begin{aligned} \Phi_s = \Phi_1 \cos\left(s\omega t - p\theta_r\right) + \Phi_5 \cos\left((6-5s)\omega t + 5p\theta_r\right) \\ -\Phi_7 \cos\left((7s-6)\omega t - 7p\theta_s\right) + \Phi_{11} \cos\left((12-11s)\omega t + 11p\theta_s\right) \ldots \ldots \end{aligned} \tag{13}$$

$$\Phi_s = 0.5 \sum \sum \Phi_n \cos\left[(k_1 \pm k_2(\frac{(1-s)}{p})) \pm k_2\theta_r \right] \tag{14}$$

$$f = \left[(k_1 \pm k_2(\frac{(1-s)}{p})) \pm k_2\theta_r \right] \tag{15}$$

As described in reference [14], the faulty and healthy squirrel-cage induction motor current is given by (16) and (17), respectively. According to reference [23], when there is a short circuit or static eccentricity in the stator, a negative sequence component appears, the amplitude of which depends on the percentage of shorted turns. As described in reference [24,25], the components due to stator failures (f_{sf}) are given by Equation (18), while according to reference [26], in the case of a healthy motor, the main components are the first and fifth harmonics. In the case of an unbalanced voltage, regardless of slip, this fault shows itself mainly in the first and third harmonics. According to reference [27], short circuits cause the components given by Equation (19). As described in reference [28], in a symmetrical stator, the CS contains the harmonics given by Equations (20) and (21), for which the harmonics determined by Equations (22) through (24) should be added, in case of asymmetry. As described in reference [29], another simple alternative for the early detection of stator faults depends on the magnitude of the negative sequence of the current, which allows us to obtain the negative impedance to be compared with the average winding impedance.

$$i_a(t) = i_A(t) = i_a(t)\left[1 + k_m \cos(\omega_f t)\right. \tag{16}$$

$$i_A(t) = I \cos\left(\omega_s t - \varphi - \frac{\pi}{6}\right) + \frac{k_m I_L}{\sqrt{2}} \{\cos\left[(\omega_s + \omega_f)t - \varphi - \frac{\pi}{6}\right] + \cos\left[(\omega_s - \omega_f)t - \varphi - \frac{\pi}{6}\right]\} \tag{17}$$

$$f_{sf} = \left[2k_0(\frac{1-s}{p}) \pm k_1\right]f_s \tag{18}$$

$$f = f_s\left[\frac{2k}{p}(1-s) \pm k_1\right] \tag{19}$$

$$f_{s1} = f_s \left| (1 - k_3) - \frac{2k_4 Q_r}{p}(1 - s) \right| \tag{20}$$

$$f_{s2} = f_s \left| (1 - k_3) + (-\frac{2k_4 Q_r}{p} + 2 + 6k_0)(1 - s) \right| \tag{21}$$

$$f_{s3} = f_{s1} - (n_1 + 1)s f_s \big|_{n1=1} = f_{s1} - 2s f_s \tag{22}$$

$$f_{s4} = f_{s2} - (n_1 + 1)s f_s \big|_{n1=1} = f_{s2} - 2s f_s \tag{23}$$

$$f_{s5} = f_s \tag{24}$$

As described in reference [30], rotor faults generate components below the supply frequency in the stator spectrum, according to Equation (25), where the first term does not contribute to increasing the supply current because it induces an MMF of zero sequence. However, the second term induces a set of three-phase currents at the supply frequency and contains a component displaced by twice the slip frequency, $2s f_s$. The fault causes a $2sp\omega_{mr}$ variation in rotor speed, causing a displacement of the lower component $(1 - 2s) f_s$ and the appearance of an upper component at $(1 + 2s) f_s$ modulated by the third harmonic of the stator flux. Other components that may appear are given by Equation (26). Because of the static, dynamic, or mixed eccentricity, the air gap is not uniform, and the forces applied to the shaft become unbalanced, causing friction between the stator and rotor. According to references [26,31,32], the eccentricity causes the appearance of harmonics whose sequence is given by (27). If the eccentricity is static, n_d is zero, while if it is dynamic, it is $1, 2, 3, \ldots$ However, according to reference [33], a difference between static and dynamic eccentricity does not always exist for all motor configurations, in addition to the fact that there are components that are not easily detectable.

$$f_s = \frac{N_r I_2}{2} \{ \cos[(3 - 2s)\omega_s t - 3p\theta_1] - \cos[(1 - 2s)\omega_s t - p\theta_s] \} \tag{25}$$

$$f_s = (1 \pm 2k_0 s)\omega_s \tag{26}$$

$$f_{ecc} = \left[2(k_0 Q_r + n_d)\left(\frac{1 - s}{p}\right) \pm v \right] f_s \tag{27}$$

As described in reference [34], mechanical faults can be classified as those that cause air gap eccentricity, load torque oscillations, or a combination of both. The first effect is due to unbalanced loads, shaft misalignment, and gearbox and bearing failures. The second effect is due to wear or failure of the bearings and to rotor imbalance caused by poor assembly, for example. The load torque oscillation component, Equation (28), affects the rotor position and stator current. The length of the air gap affects the permeance, flux density of the air gap, and MMF, which ultimately modulates the stator current signal. When there is air gap eccentricity, that failure can vary with time and the angle of the circumference θ, so, in the case of dynamic eccentricity, the length of the air gap is a function of θ and t, according to Equation (29). The use of $\omega_r t$ in the last equation provides an expression for the static eccentricity. From this last expression, it is deduced that the dynamic eccentricity produces components given by (30) in the signal spectrum. In addition, the modulation of the phase and the amplitude occur at the same rotor frequency.

$$T_T(t) = T_o + T_{osc} \cos(\omega t) \tag{28}$$

$$g_{de}(\theta, t) \approx g_0(1 - \delta_d \cos(\theta - \omega_r t)) \tag{29}$$

$$f_s \pm f_r \tag{30}$$

3. Signal Processing Techniques Applied to Wind Turbine Failure Detection

Initially, the study of the signals was carried out in the time-amplitude plane and was based on the variation of the waveform in addition to the calculation of parameters such as the average value,

peak value, interval between peaks, standard deviation, crest factor, root mean square value, kurtosis, and skewness [35,36]. According to reference [37], synchronizing the sampling of the vibration signal with the rotation of a gear and evaluating the average of several revolutions provide a signal called the synchronized time average, which is expressed by Equation (31). This equation makes it possible to accurately approximate a periodic signal and obtain the vibration pattern (including any modulation effects) of the gear teeth of a gearbox. However, according to the author, this method requires repeating the analysis for each gear. As described in reference [38], the most advanced proposed methods for the analysis in the time domain apply time series models to the signal, among which are those of auto regression (AR) and the autoregressive moving average (ARMA), which are applied in references [39–41]. Currently, the parameters used in the analysis of the current signal in the time domain can be used for the detection and diagnosis of faults using artificial intelligence models [42]. Thus, in reference [35], the eight parameters of the current signal in the time domain are the input variables of a three-layer artificial neural network (ANN) used to predict the remaining useful life (RUL) of the bearings of the gearbox of a WT.

$$g(t) = \sum_{k_0=0}^{k_0} A_{k_0}(1 + a_{k_0}(t)) \cos{(2\pi k_0 f_{te} t + \varnothing_{k_0} + b_{m_0}(t))} \tag{31}$$

As described in reference [43], the complex sinusoidal and cosine signals in the time domain can be better analyzed using their frequency components obtained with the Fourier transform (FT). According to references [38,44], the analysis in the frequency domain allows us to obtain information that is not available in the time domain, for example, knowing the origin of the signal, the phase modulation, and the moment at which the components arise. When the signals are stationary, their frequency spectrum is constant over time, so the analysis can be performed using the FT. For example, reference [45] determines the frequencies associated with the DFIG faults of WTs by applying the fast Fourier transform (FFT) to the current signal of the electric generator, but during periods of steady-state, that is, when the speed is constant.

When the signals are transient and not periodic, such as during startup or load variation or under wind speeds with stochastic behavior, the spectrum is oscillatory. Under these conditions, the FFT and analysis in the frequency domain are not sufficient, so it is necessary to resort to other techniques that allow analysis in the time-frequency domain, such as the short-time Fourier transform (STFT), wavelet transform, Wigner–Ville distribution (WVD), and Hilbert transform (HT) [42,46,47].

One of the first alternatives used to overcome the disadvantages of the FT was the windowing technique proposed in 1946 by Dennis Gabor, which consisted of applying the FT to only a small section of the signal at a time. This methodology is the origin of the STFT, which allows the signals to be represented as a function of time and frequency. For this, the total signal time is divided into shorter time intervals [48,49]. The signal is multiplied by a window function, Equation (32), and for each resulting interval, the discrete time FT (DTFT) is given by (33) and (34). For a fixed time (*n*) of analysis, the DTFT is known as the STFT, where (32), which is a sequence of DTFTs, is a periodic function of frequency ω and period 2π. There is a different spectrum in each window, and by analyzing all the intervals as a whole, the variation in frequency over time can be observed. When, instead of studying the spectrum at a certain time, one wishes to study a specific frequency, then the windowing process is carried out in the frequency domain. The quality of the results depends on selecting the window that minimizes losses due to spectral leakage and reduces the amplitude of the main and secondary lobes [50].

$$x_{\bar{t}}(m) = x(m)h(\bar{t} - m) \tag{32}$$

$$X_{\bar{t}}(e^{j\bar{\omega}}) = \frac{1}{\sqrt{2\pi}} \int e^{-j\bar{\omega}m} x_m(m)h(\bar{t} - m)dm \tag{33}$$

$$X_{\bar{t}}(e^{\bar{j\omega}}) = \sum_{m=-\infty}^{\infty} x(m)h(\bar{t}-m)e^{-\bar{j\omega}m} \tag{34}$$

$$X_{\bar{t}}(e^{\bar{j\omega}}) = (x[t]e^{-j\omega t}) * \omega[t]\Big|_{t=\bar{t}} \tag{35}$$

As described in reference [38], the STFT has resolution problems due to signal segmentation; one of the alternatives to overcome this limitation is the WVD. This distribution is one of the most popular ones since, unlike the STFT, it is not based on signal segmentation, providing better resolution in both the time domain and the frequency domain. According to references [47,51], given a signal *s(t)* in the time domain, the WVD is defined by (36), while starting from the frequency spectrum of *s(t)*, it is given by (37). It can be assumed that using the WVD means dividing the signal into two equal parts in relation to a time *t*, with the right part overlaid over the left part, which means that when the signal is null before or after *t*, then the signal is zero in *t*. The correct average is obtained only when the signal can be separated into a component that is a function of time only and another function of frequency. A signal that is not zero at time zero or a signal with frequencies without the existence of a spectrum indicates the presence of interference or cross terms. As described in reference [34], a sinusoidally modulated amplitude current signal has the same components as in (30), which means that when $f = fr$, in the case of faults due to torque oscillations and eccentricity, the use of classic spectral analysis (SA) does not allow us to distinguish between amplitude and phase modulation since the modulation indices are small. However, the use of the WVD does allow us to distinguish these faults using Equation (38).

$$W(t,\omega) = \frac{1}{2\pi} \int_{-\infty}^{\infty} s^*(t - \frac{1}{2}\tau)s(t + \frac{1}{2}\tau)e^{-j\tau\omega}d\tau \tag{36}$$

$$W(t,\omega) = \frac{1}{2\pi} \int_{-\infty}^{\infty} S^*(\omega + \frac{1}{2}\theta)S(\omega - \frac{1}{2}\theta)e^{-jt\theta}d\theta \tag{37}$$

$$f_s \pm \frac{f_r}{2} \tag{38}$$

The small magnitude of the components associated with the faults makes their extraction difficult. To overcome this drawback, one of the most suggested techniques is to demodulate the signal amplitude. For this, according to reference [52], the best option is to use HT due to its strength to handle noise. According to that report, when there are no faults, the amplitude of the envelope is constant over time, and its variance is zero. Otherwise, if the variance is greater than a pre-established threshold level, some type of asymmetry exists.

According to reference [53], the HT of a signal is the relationship between the real and imaginary parts of the FT of said signal. Similarly, the function of time obtained by the Fourier inverse is a complex function called the analytical signal, the imaginary part of which is the HT. The analytical signal can be represented as a phasor whose amplitude and rotation speed vary over time, according to Equation (39), implying that, given a function in the time domain, in addition to the amplitude, one can also obtain the components that modulate the frequency or phase, $\tilde{a}(t)$. In the HT, the amplitude function is the envelope of both the real and the imaginary parts and represents the modulated signal plus *dc* compensation. In the case of oscillating functions, the direct analysis in the frequency domain of the periodic variations over time of the components introduced by some type of anomaly does not provide enough information. However, if a bandpass filter is used in the region containing the components that modulate the CS and its envelope is obtained, the frequencies associated with the faults can be easily identified. Additionally, since the magnitude of the envelope can be plotted on a logarithmic scale, exponential decays can be converted into straight lines to detect low-level peaks.

This is the reason why the demodulation of the amplitude of the current signal is one of the most used techniques for the detection and diagnosis of faults in rotating electrical machines using SA.

$$A(t)e^{j\omega(t)} = a(t) + j\widetilde{a}(t) = a(t) + \frac{1}{\pi} \int_{-\infty}^{\infty} a(\tau)\frac{1}{t-\tau}d\tau \tag{39}$$

According to reference [54], mathematically, the HT along with its FFT are given by (40). The composition of the analytical signal and its amplitude, phase of the envelope, and instantaneous frequency can be obtained from Equation (39). Both positive and negative components have a 90° offset, and Equation (41), according to the Park transform, takes the same form after applying HT as Equation (17). From this, it follows that the characteristic frequencies are f_m and $2f_m$, there being a dc component in f_m, $2f_m$, $2(f_m + f_1)$, etc. According to reference [55], when some type of failure occurs in the multipliers, a new impulse appears in the original spectrum or phase spectrum. For this reason, prior to using the FFT to obtain the spectrum, demodulation is applied (using the HT) to the current signal, demonstrating the effectiveness of this technique in the detection and diagnosis of pinions and broken teeth in the gearbox of a WT.

$$\overline{x}(t) = \frac{1}{\pi} \int_{-\infty}^{\infty} \frac{x(\tau)}{t-\tau}d\tau = x(t) * h(t) = x(t) * \frac{1}{\pi t} \tag{40}$$

$$i_{sq} = i_{sq0} + i_{sqv} \sin\left(\omega_m t + \varphi_{sqv}\right) \tag{41}$$

According to reference [56], due to the operating characteristics of the WTs, the resolution of the STFT, in both the time and the frequency domains, is limited. The wavelet transform has the capacity to analyze variations in the signal in the coupled time-frequency domain. However, this process depends strongly on the chosen function and requires prior knowledge of the signal used, while empirical mode decomposition (EMD) lacks a theoretical foundation and requires extreme interpolation. In this context, the author proposes a new method to detect the failures of the gearbox of the WTs, which is based on first demodulating the stator current signal of a DFIG using the HT and then applying a signal resampling algorithm based on the generator rotation frequency, such that the resampled envelope has a constant phase angle range.

While the FT decomposes a signal into a set of waves of different frequencies, the wavelet transform transforms a signal contained in space to a time-scale region using an infinite set of functions called wavelets and defined according to Equation (42), called the wavelet mother. Similar to the FT, the continuous wavelet transform (CWT) represents the sum of the products of the signal multiplied by each of the wavelets, as shown in Equation (43). The characteristics and properties vary according to the type of mother wavelets or wavelet families, among which we mention the Haar wavelet, Daubechies wavelets, symlets, coiflets, biorthogonal wavelets, reverse biorthogonal wavelets, Meyer wavelets, discrete approximations of Meyer wavelets, Gaussian wavelets, Mexican hat wavelets, Morlet wavelets, complex Gaussian wavelets, Shannon wavelets, frequency B-spline wavelets, and complex Morlet wavelets. Unlike the STFT, wavelet transformation allows the window measurement to be varied in such a way that a wide window can be used when information about low frequencies is required and narrow windows when it is necessary to analyze high frequencies since the latter are detected better in the time domain, while low frequencies are more accurately analyzed in the frequency domain. This property means that wavelets can be used in the SA at different frequencies and resolutions of both stationary and transient signals [48].

$$\Psi_{a,b}(t) = \frac{1}{\sqrt{a}}\Psi\left(\frac{t-b}{a}\right) \tag{42}$$

$$C(a,b) = \int_{-\infty}^{\infty} f(t)\Psi(a,b)dt \tag{43}$$

As described in reference [57], techniques such as the CWT and discrete FT have disadvantages when the analysis is carried out with small loads and close to the synchronism speed. According to this author, a more effective method for detecting faults and analyzing the evolution of their severity is

to use a Kalman filter, which is computationally more efficient. Since the CWT requires considerable computational effort and generates too much data, an alternative is to filter the signal iteratively in such a way that each frequency band obtained is again decomposed and so on until we obtain several high-resolution frequency components, on which we perform the analysis. In other words, the alternative is to discretize the parameters of both scale and time, leading to the discrete wavelet transform (DWT), also called multiresolution analysis [58]. According to reference [59], calculating the coefficients throughout the scale increases the calculation time, while according to reference [60], it can be shown that the CWT is not useful for detecting faults or torque variations; therefore, the use of the DWT is preferable. According to that report, the signal must first be decomposed by the CWT with a Daubechies 8 (Db8) mother function, and then the FFT is used to analyze the spectrum components.

In reference [61], the components of the fundamental frequency and harmonics due to eccentricity, slots, and other unknown causes, including environmental noise, determine the CS. However, these components are not those related to the generalized bearing roughness; therefore, to detect this type of failure, that work proposes to eliminate the mentioned components by filtering the generator stator signal from a WT using the DWT based on the coiflet function. In addition, the signal is also broken down by wavelets into several segments until the components associated with bearing failures are obtained. As described in reference [62], in regard to detecting broken bars, the main problem with steady-state analysis is that the frequency separation depends on inertia, which means that for small loads, the separation decreases to a point where the frequencies associated with the broken bars cannot be distinguished, so those authors propose processing the signal using wavelets. The current signal of an induction motor is also broken down by wavelets for the detection of broken bars under different load conditions. According to the authors, the high-order Daubechies family behaves as an ideal filter and partially avoids overlap between frequency bands. In reference [63], the current signal of an induction motor is also segmented by wavelets to detect broken bars under different load conditions. According to the authors, the high-order Daubechies family behaves as an ideal filter and partially avoids overlapping between frequency bands. According to reference [16], the use of wavelets makes it unnecessary to know the slip, and in reference [20], a diagnosis of broken bars is proposed based on the current signal and the transformation of wavelets, without using the slip.

As described in reference [64], it is possible to identify the incipient presence of broken bars by applying the DWT with the Daubechies-44 family. Furthermore, since the transient state of the induction motor can offer very useful information for the detection of electromechanical faults, such as the dynamic eccentricity, the signal is sampled during startup. The detection of failures of loads coupled to the induction machine using the MCSA has also been extensively studied, such as in reference [65], where this methodology is used to detect gearbox failures caused by broken gears or broken teeth. The use of GCSA for this purpose in WTs has not received the same attention, especially in regard to studies based on real data.

In the time-frequency analysis, both variables are dependent, and according to the Heisenberg uncertainty principle, it is not possible to know exact values but only intervals [66]. The autocorrelation and power spectrum function does not provide all the necessary information, such as phase coupling or bicoherence, whereas the STFT has the drawback of temporal resolution. For this reason, in the case of non-Gaussian and nonlinear signals and signals whose spectrum is made up of a large number of frequencies, SA must be implemented using high-resolution or higher-order-spectrum (HOS) techniques [67]. Among these techniques is an approach using the bispectrum, which, being a complex number, consists of magnitude and phase. The bispectrum can be used to analyze the relationship between the frequencies of two sinusoids and the result obtained due to the modulation between them. For each set of three frequencies, the signal power and phase are calculated; if the phase shift between the two sinusoids tends to zero, then both have the same origin. Otherwise, the phase shift provides an indication of failure [68].

According to reference [69], given a signal $X(K)$, its second-order statistical characterization can be represented by the autocorrelation and power spectrum function. For the same signal, with zero

mean, its third-order moment is given by (44). If the signal is not stationary, Equation (44) depends on three parameters (k, τ_1, τ_2), while for stationary signals, the function contains only τ_1 and τ_2. The FT of the second-order momentum is the power spectrum that we have seen previously, while the bispectrum is the double FT of the third-order momentum and is defined by Equation (45). The degree of coupling between frequencies of different phases is measured by the bicoherence index, Equation (46), whose magnitude varies from zero to one. The greater the value, the greater is the coupling [70]. According to reference [26], the bispectrum technique allows us to represent the FFT of both the phase and the amplitude of the signal. Since the magnitude of the dominant component is a function of the level of the fault, when this technique is applied to the current of induction motors, the spectrum of the current signal allows the detection of electrical faults. The theoretical and mathematical foundations of HOSs are addressed in reference [71–75].

$$c_{3,x}(k, \tau_1, \tau_2) = c_{3,x}[x(k)x(k + \tau_1)x(k + \tau_2)] = E[x(k), x(k + \tau_1), x(k + \tau_2)] \tag{44}$$

$$B(f_1, f_2) = E[X(f_1)X(f_2)X \times (f_1 + f_2)] \tag{45}$$

$$bic(f_1, f_2) = \frac{B(f_1, f_2)}{\sqrt{P(f_1)P(f_2)P(f_1 + f_2)}} \tag{46}$$

Other HOS techniques used are frequency estimators based on eigen analysis. This methodology divides the RM autocorrelation matrix into two vector subspaces, one representing the signal and another representing noise, as shown in Equation (47). The order of the matrix and its eigenvalues are given by (48). Among the frequency estimators developed based on this methodology, multiple signal classification (MUSIC) and root MUSIC can be mentioned, which, as addressed in [76], are high-resolution models that allow for the detection of frequencies in signals with low signal-to-noise ratios.

$$d(n) = \sum_{k=1}^{s_i} A_k e^{(j2\pi n f_k + \varnothing_k)} + e(n) \tag{47}$$

$$M = \{\lambda_1 + \sigma^2,\ \lambda_2 + \sigma^2, \ldots\ldots,\ \lambda_L + \sigma^2,\ \sigma^2,\ \ldots\ldots \sigma^2\} \tag{48}$$

As described in reference [76], although the relevant techniques generally deal with the detection of a fault, in induction motors, it is most likely to find the presence of several faults, and for its detection, a high-resolution model is proposed that combines a bank of infinite impulse responses and MUSIC. According to the authors, this method is capable of detecting broken bars, imbalance, and defects in the outer bearing race. Another approach that MUSIC uses is described in reference [77]. Although signal sampling is generally performed during machine operation and in some approaches during startup, in that work, signal sampling is performed when the machine is disconnected from the network since, according to reference [75], as the terminal voltage is produced by the rotor currents, the presence of broken bars is reflected in the spectrum of the stator voltage. On the other hand, according to reference [78], the disadvantage of MUSIC is that by increasing the correlation matrix to find more frequencies, the required computational effort increases. To overcome this drawback, that work proposes applying an algorithm similar to the zoom-FFT (ZFFT) method that focuses on certain frequencies regardless of the total frequency range while applying zoom-MUSIC (ZMUSIC). According to the authors, very good results are obtained with the proposed method, comparable to those obtained with ZFFT but requiring less sampling time and less memory capacity.

Other models used for HOS fault monitoring and detection include estimation of signal parameter via rotational invariance technique (ESPRIT) and PRONY. ESPRIT belongs to the subspace parametric spectrum estimation methods expressed by Equations (52) and (53) [79], whereas according to reference [80], the PRONY method is used to model the sampled data of a signal using a linear system of complex exponential functions. As described in reference [81], the extensive use of the power converter when the DFIG works below the synchronous speed causes the current to have a high

content of interharmonics that can cause resonance, in addition to damage to capacitors, insulation, control elements, and protection. According to the authors, the identification of these harmonics can be performed using the PRONY and ESPRIT methods, although the latter has a lower resolution than the former.

According to reference [82], to overcome spectral leakage, high-resolution analysis should be applied, but since this implies a longer sampling time, the spectrum varies both in frequency and in amplitude, making diagnosis difficult. From this, it can be deduced that there are no stable conditions that are required to apply the FFT and that its use does not guarantee the identification of the frequency components. The DWT allows for better spectral resolution. However, in general, the proposed signal techniques are not efficient at low slips, such as 1%. Based on the foregoing, reference [82] proposed using ESPRIT in combination with an improved Hilbert's modulus method, which was successful in detecting broken bars even with a slip as small as 0.33%, using only the one-phase signal and short sampling time. When the same experiments were performed using MUSIC, satisfactory results were not obtained, demonstrating the superiority of ESPRIT.

Another technique that has been widely used to diagnose faults in electrical machines is Park's vectors. According to Fortescue's theorem, a triphasic system can be represented as the sum of the components as a zero or homopolar, positive sequence and negative sequence, as expressed in Equation (49) [83]. For three-phase induction motors, the three phases can be represented in the 2D *dq* plane with Equations (3) and (4), known as Park vectors or Concordia patterns. In the absence of faults, the Park vectors have components given by (50) and (51), whose graph is circular and centered on the origin, while when there are faults in the stator and/or rotor, the graph is deformed and takes on an elliptical shape [84–89].

$$
\begin{bmatrix} I_a \\ I_b \\ I_c \end{bmatrix} = \begin{bmatrix} 1 & 1 & 1 \\ 1 & a^2 & a \\ 1 & a & a^2 \end{bmatrix} \begin{bmatrix} I_a^0 \\ I_a^+ \\ I_a^- \end{bmatrix}
\tag{49}
$$

$$
i_d = \frac{\sqrt{6}}{2} I_s \sin \omega t
\tag{50}
$$

$$
i_q = \frac{\sqrt{6}}{2} I_s \sin(\omega t - \frac{\pi}{2})
\tag{51}
$$

4. Materials and Methods

This research work has two parts. In the bibliographic part, emphasis has been placed on the presentation of the theoretical foundations, mathematical models, and existing proposals for some of the most used methodologies for the detection and diagnosis of failures in WTs. The second part is a field investigation, with the purpose of verifying the effectiveness of the analyzed models to determine the status of WTs in operation. The mentioned WFs were installed approximately 20 years ago, and the one where the measurements were made consists of 33 WTs of brand NEG Micon. The electric generator used by the WTs is a SCIG with two windings, one of small power (200 kW) for low speed and the other of a higher power (900 kW) for higher wind speeds (see Table 1). As at the time of testing, the wind speed was high, and measurements were made on the highest-power generator (see Figure 1).

**Table 1.** Technical characteristics of the WT and electric generator.

Brand	NEG Micon
Model	NM 52/900
Rotor diameter	52.2 m
blades	3
Power	900 kW
Power control	Stall control
Drive train	Gearbox type: Planetary-Parallel Transmission ratio: 1:67.5 Main bearing: spherical rollers Cooling system: refrigerant, heat exchanger and pump
Electric Generator	Type: SCIG Speeds: 750/500 rpm Poles: 4/6 Power: 900 kW/200 kW Voltage: 690 V/50 Hz Cooling system: water
Coupling to the power grid	Smooth, using thyristors
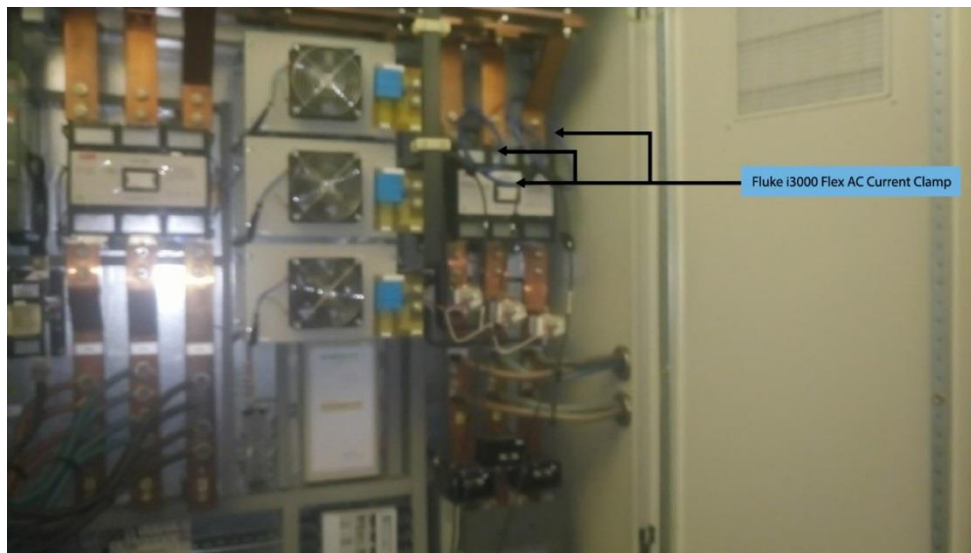
Figure 1. Location of the current clamps on the WT power panel.

For measurements, in addition to the Fluke i3000s flexible clamps, a Pico Technology unit, model PicoScope®4424, was used, which must necessarily be connected to a computer in which software has previously been installed to be able to acquire the signal. Data were acquired by applying a sampling rate of 10 kHz over 2s (representing 20,000 data points per sample). This measurement was made continuously for approximately 10 min. The processing of the data and the application of the various SA techniques were performed in MATLAB r2019b software.

5. Results and Discussion

By applying the FT to the current signal of the generator under study, Figure 2a,b are obtained for one and three phases, respectively. In the graphs, harmonics with frequencies of 40, 42, 46 and 56 Hz can be distinguished, which, according to references [42,76,90], are related to stator failures, broken bars, and phase imbalance. In addition, as described in reference [42], rotor failures are manifested by harmonics of the fundamental frequency (3, 5, 7, etc.), which reinforce the indications of bar failure.

(**a**)

(**b**)
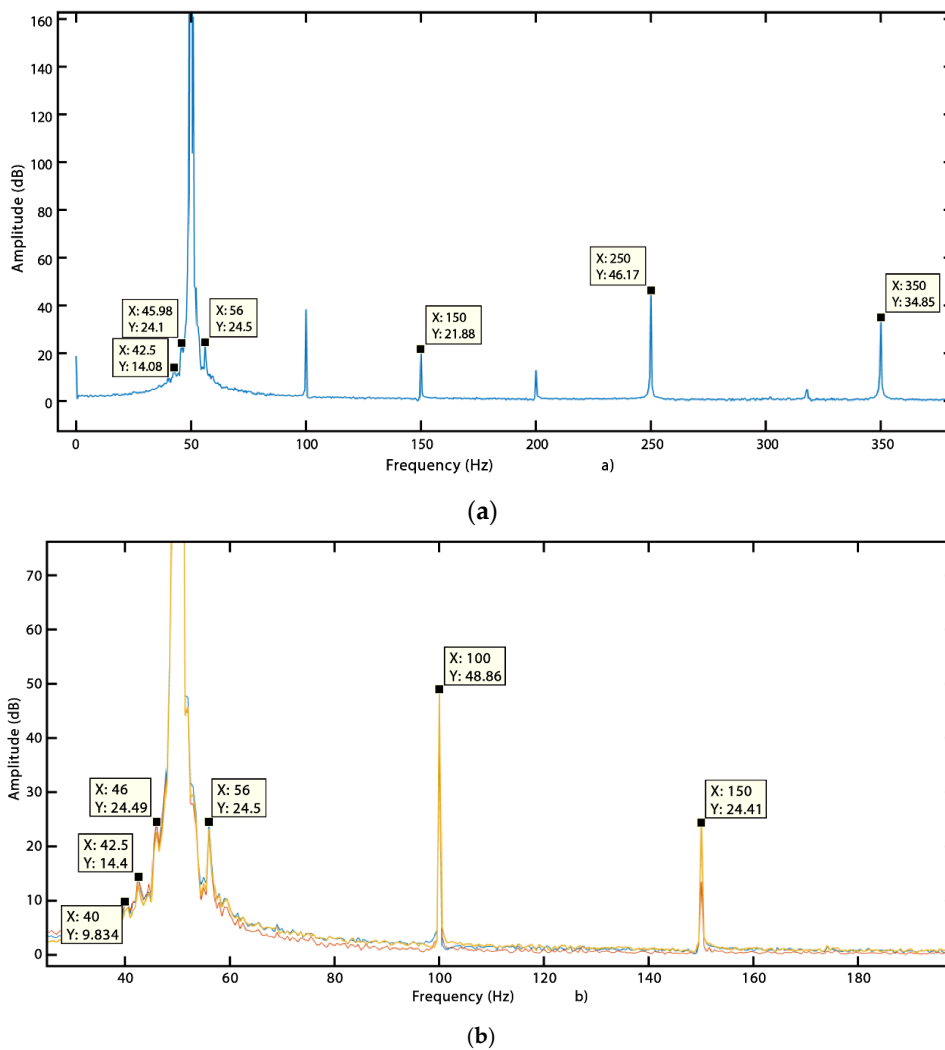
Figure 2. FT of the WT current signal. (**a**) One phase and (**b**) three phases.

The frequency components are very close to the central frequency, and depending on the window used, the width of the lobes can be very large, and the identification of faults by means of the FFT is difficult, making it necessary to resort to other variables and techniques such as the power spectral density (PSD) [91]. In MATLAB, we obtain an improved version of the PSD, which is shown as a Welch periodogram (see Figure 3). In this approach, by definition, MATLAB applies the Hamming window and displays the part of the graph corresponding to the real values. Unlike the case of the classic FT, in the spectrum obtained by the Welch periodogram, a greater number of frequency peaks can be distinguished, such as 30, 46, 54, 63, 124, 165, 261, 451, 534, 575, and 781 Hz. Although the composition of the spectrum is uniform, there are differences in the magnitudes of the components. These differences can also be observed when comparing the three phases of the generator (see Figure 3b).

(a)

(b)
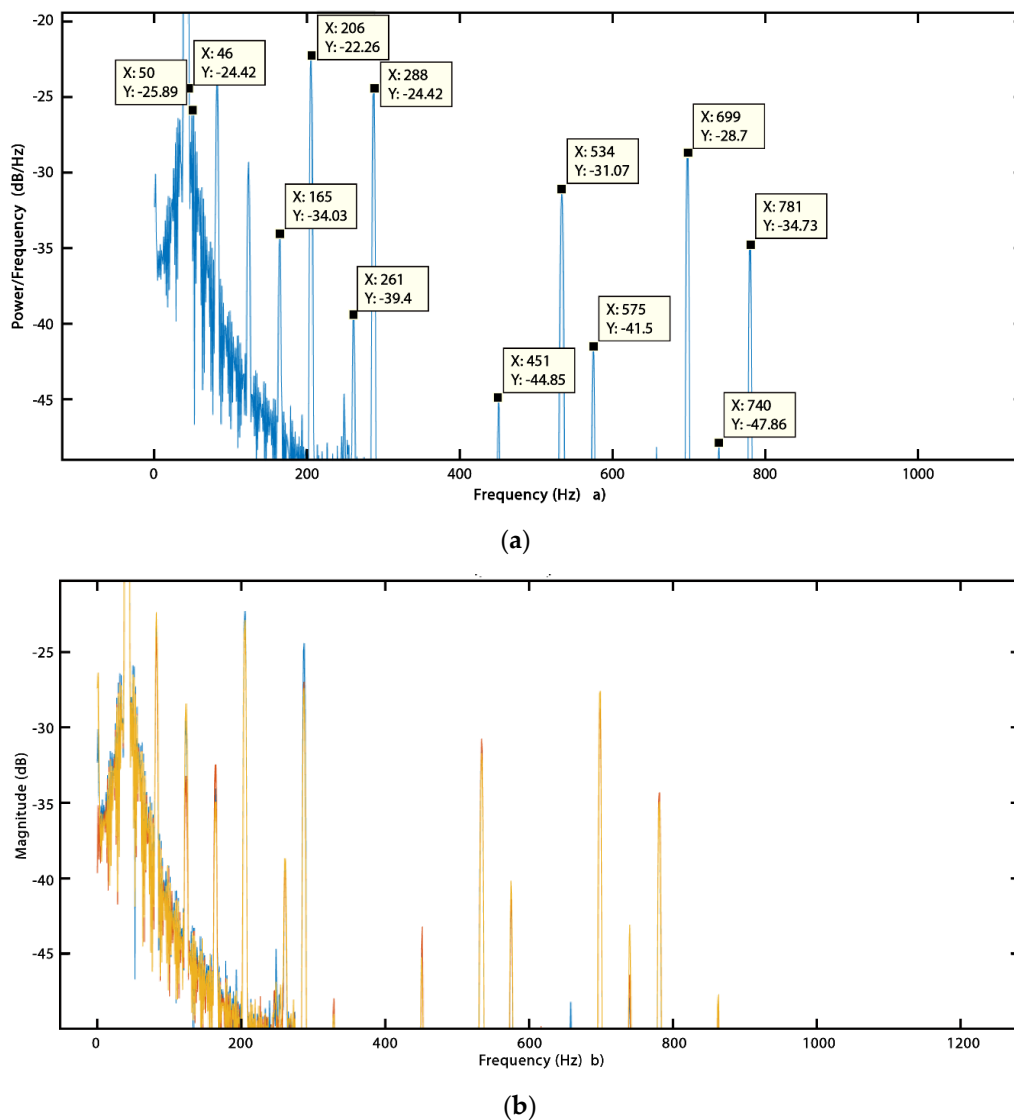
Figure 3. PSD applying Welch's periodogram. (**a**) Phase A and (**b**) three phases.

Another alternative to overcome the drawbacks mentioned so far is the proposed methods to eliminate frequencies that are not of interest so that it is easier to identify the components sought. In this context, one option is the technique known as cepstrum analysis, which calculates the inverse FT of the signal spectrum on a logarithmic scale. Failures alter the rotor speed and magnitude of the components, creating new frequency components that have their own harmonic families. The cepstrum provides an average of each of these families displayed as a single line with their respective harmonics bands. Identifying the frequency of each frequency also allows for the separation of signals that have been combined due to convolution [53,92].

By applying cepstrum analysis and selecting the appropriate scale for the axes, Figure 4 is obtained. Several families of components close to the fundamental wave can be more clearly distinguished than before. For our case, the harmonic families separated by 200 ms that are equivalent to 5 Hz are easily visible. These frequencies are consistent with a fault attributed to broken bars, as was deduced with the previous techniques. Other types of mechanical failures associated with these frequencies are imbalances of the blades and bearings of the generator, which, according to reference [93], are manifested by frequencies of 10 and 5 Hz, respectively. Although there is considerable similarity in the spectrum of the three phases obtained with this technique, differences in the composition of the spectrum and the magnitude of the components can also be highlighted, providing another indication of failure.
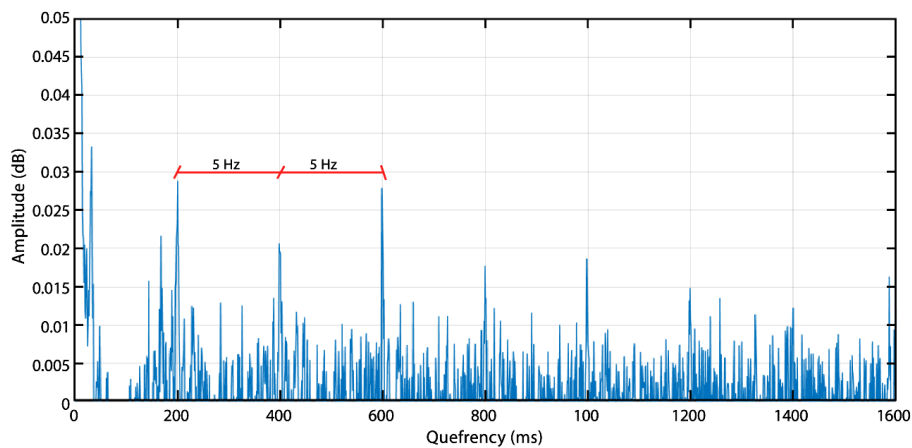
Figure 4. Signal cepstrum of the electric generator.

As we have been able to verify from the techniques used so far, time-domain analysis does not provide the frequency spectrum, while the analysis in the frequency domain does not provide the moment at which the components are produced. By applying the algorithm of reference [94] to calculate the STFT in MATLAB, Figure 5 is obtained. Parts a and b of this figure emphasize how both the fundamental frequency and its components, which remain invariant over time, stand out in terms of their energy (yellow color). Part b reveals harmonics very close to the fundamental (green and orange color), which correspond to the frequencies of 10 and 5 Hz mentioned above.

(**a**)

(**b**)
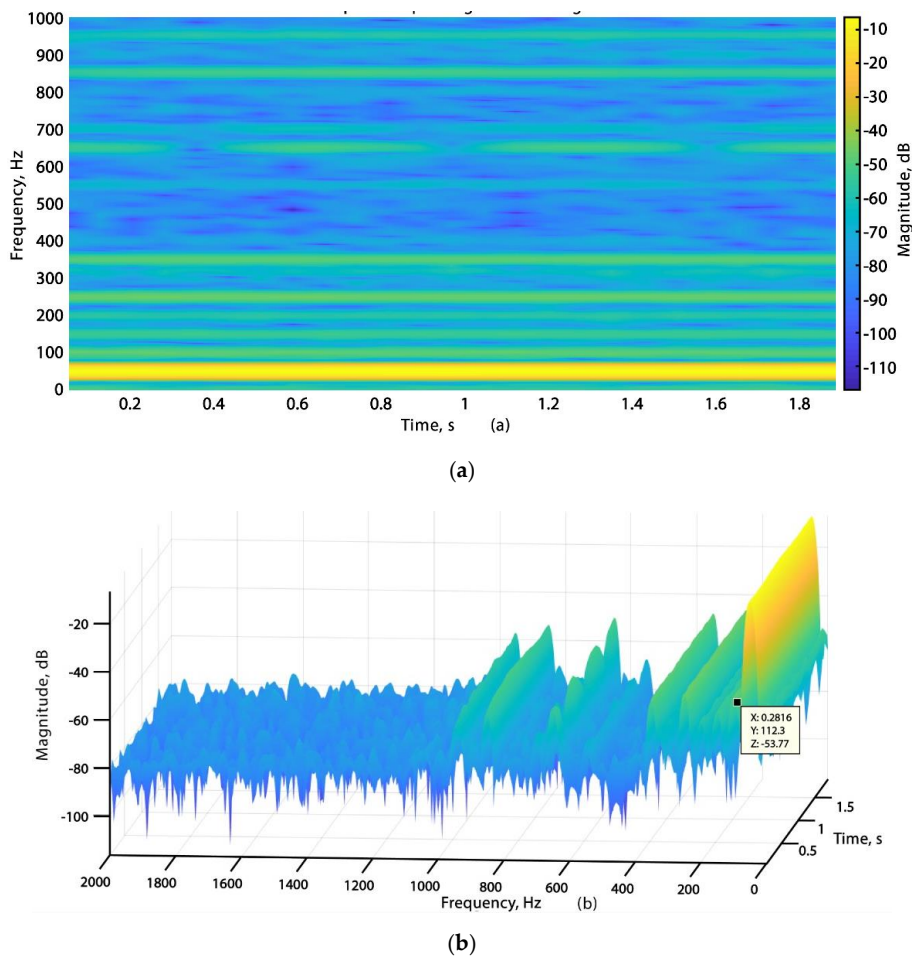
Figure 5. Amplitude spectrogram of the SCIG. (**a**) 2 dimensional STFT, (**b**) 3 dimensional STFT.

From a conceptual point of view, the STFT is one of the most important techniques and serves as the basis for other signal processing techniques. However, its main disadvantage is that it uses the same window width for the entire signal, resulting in the resolution in the time and frequency domain being constant and only one frequency band being known. If the window is wide, a good resolution is obtained in time, but a poor resolution is obtained in the frequency domain, whereas when the window is narrow, the opposite occurs. Therefore, if the frequency components are well separated, a good resolution over time may be preferred, whereas when the components are close together, the frequency resolution is prioritized. The STFT is suitable for the analysis of quasistationary signals (stationary at the window scale), which do not precisely represent the behavior of real signals. Another disadvantage is that there are no orthogonal bases for the STFT, so it is difficult to find a quick and effective algorithm to calculate it [45,65].

According to reference [47], the STFT is positive in all parts and fulfills the positivity requirement, but regardless of the selected window, it does not provide adequate resolution to distinguish the components, nor does it manage to show the instantaneous frequency that can be obtained by the WVD. However, the WVD does not meet the positivity, global average, and finite support requirements. As described in reference [38], one of the main disadvantages of bilinear distributions, such as the WVD, is the interference terms formed by the transformation, which makes interpretation difficult and prevents identifying the true components. To correct this disadvantage, distributions such as the Choi–Williams distribution, pseudo-Wigner–Ville distribution (PWVD), and smooth pseudo-Wigner–Ville distribution (SPWVD) are used [95].

Applying the SPWVD to the WT signal under study, Figure 6 is obtained. The 50 Hz frequency (yellow color) and its harmonics stand out, and—as with the previous techniques—components including 5 Hz can be distinguished along with the fundamental wave. Despite this advantage, in Figures 5 and 6, the disadvantages of the STFT and WVD mentioned by references [38,47] can respectively be seen.
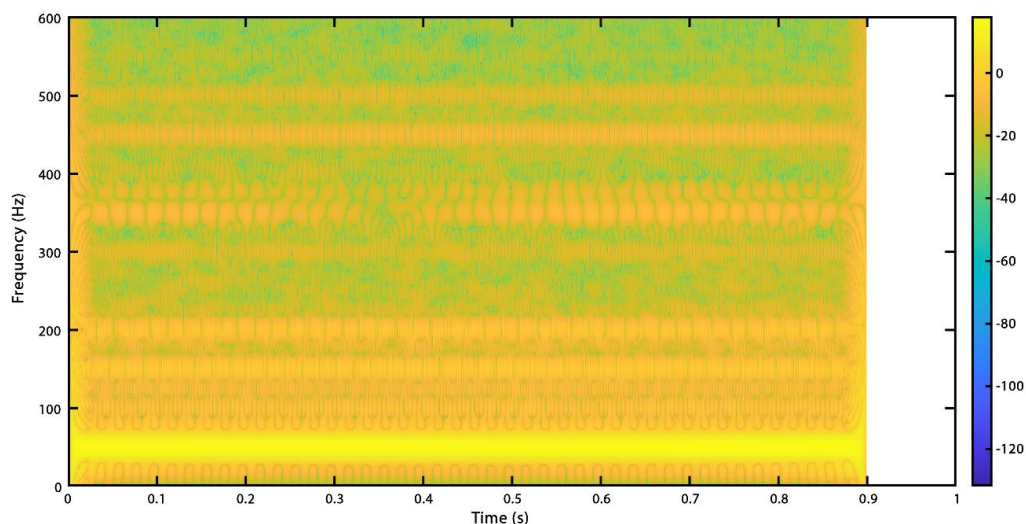

Figure 6. Smoothed PWVD.

According to reference [96], when the carrier signal frequency is on the order of kHz, bearing failures cannot be detected. However, by applying envelope analysis at the lower frequencies, detection is possible. This is the foundation on which techniques such as the shock pulse meter (SPM) and spike energy are based. HT demodulation, either directly to the current signal or to the Park transformation, is used to detect various types of rotor and stator faults, such as broken bars and inter-turn short circuits. In general, signal demodulation is usually the first phase, prior to the application of other mathematical models that are used to improve detection and diagnosis [84,85,97,98]. By applying the HT to our signal, Figure 7a is obtained, and we can distinguish the real and imaginary parts.

Taking this last part and calculating the PSD, the spectrum of Figure 7b is obtained, which is similar to those obtained using the FFT and Welch's periodogram. However, the components associated with broken bars cannot be distinguished, as it was done with the previously applied techniques.
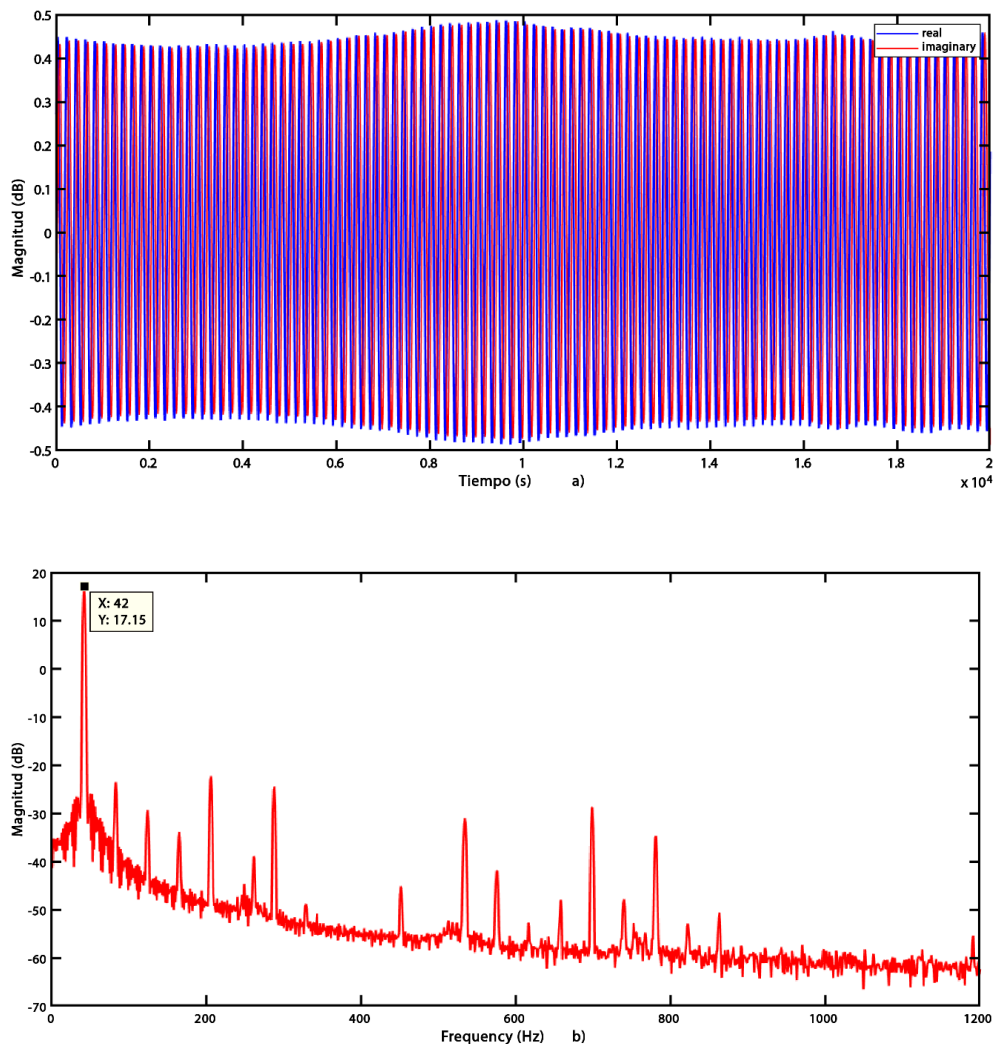

Figure 7. HT for the electrical generator signal. (**a**) Real and imaginary part of the signal, (**b**) HT PSD using the FFT.

According to reference [99], in regard to systems with multiple components, such as WTs, the approach described in reference [54] does not work because the noise processed by the HT generates spurious amplitudes at negative frequencies. To avoid this drawback, according to reference [99], the HT should not be applied directly to the signal but to each of the members of an empirical decomposition of the signal in the IMF, obtained by means of the method called sieving. By applying this methodology to the SCIG signal, Figure 8 is obtained. For our case, the MATLAB algorithm breaks down the signal into seven IMIs (Figure 8a), and proceeding as in reference [55], the HT of the first IMF is obtained (Figure 8b), to which other techniques can be applied, such as the FFT (Figure 8c). In this last figure, the components associated with broken bars are much more evident.
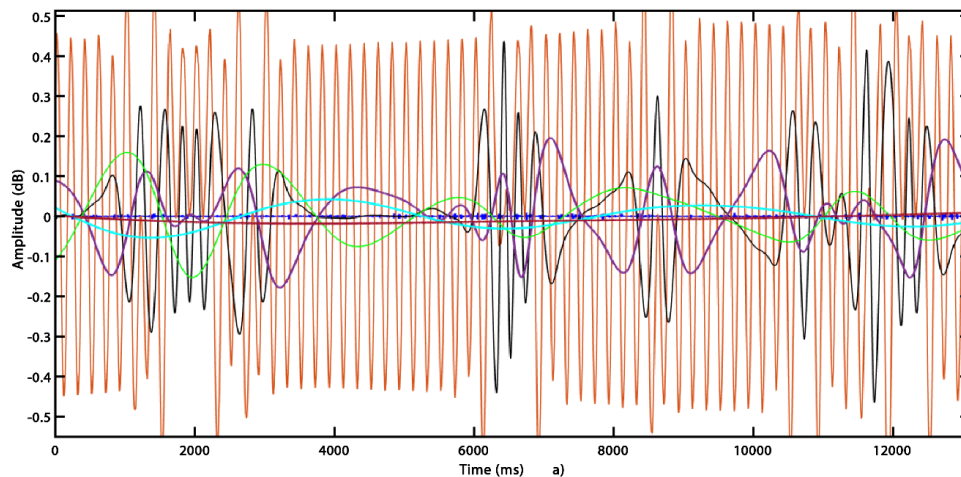
(a)
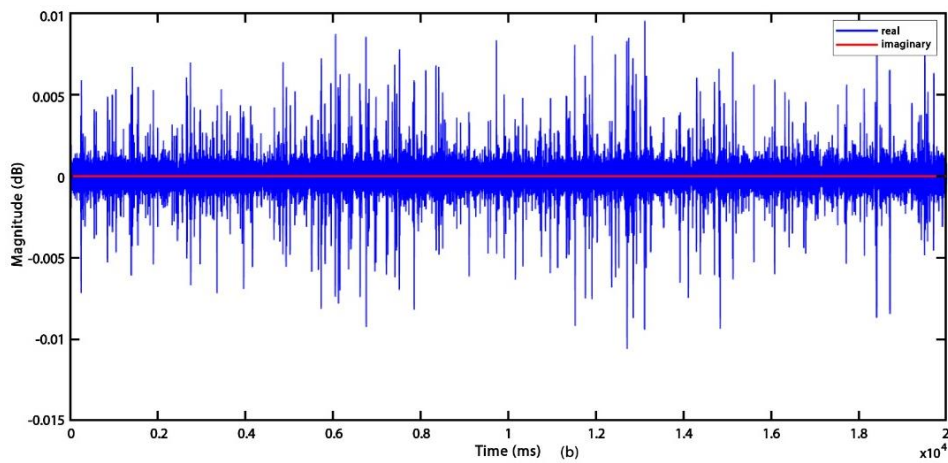
(b)
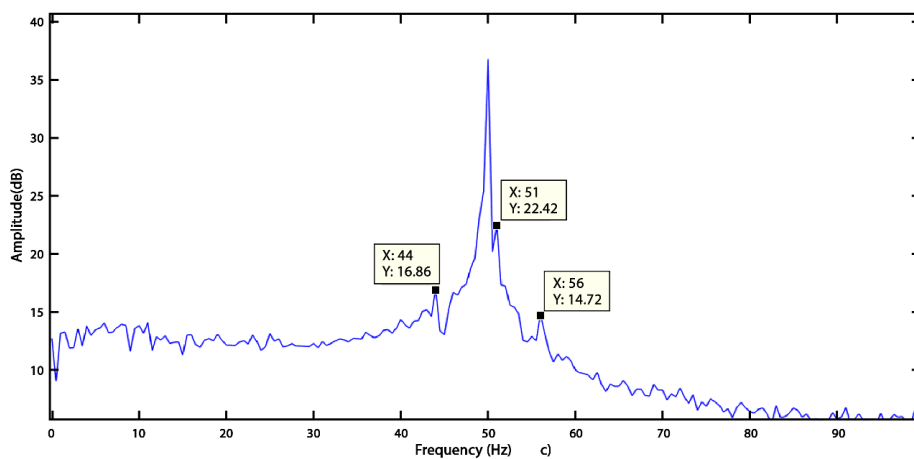
(c)

Figure 8. (**a**) Signal IMF, (**b**) HHT for the 1st IMF, (**c**) FFT of the 1st IMFs.

According to reference [42], when the generator is directly coupled to the grid using closed-loop controllers, there is no manual control over the frequency or the terminal voltage. This control system affects the behavior of the generator signal, and for fault diagnosis, it is necessary to use techniques for transient states. For this reason, the author proposes to first filter and decompose the current

signal of a SCIG using the DWT and then use the STFT to analyze the evolution over time of the frequency of interest. This allows detecting not only stator and rotor failures but also their location and identification. A similar approach to detect SCIG failures using the current signal is presented in [100]. According to this study, due to its flexibility in the analysis of the evolution of the different frequencies of a signal during transient phenomena, the wavelet transform is the most used signal processing technique for fault diagnosis. However, the author agrees in stating that the DWT cannot analyze the evolution over time of each frequency band in which the signal decomposes, which can be solved by applying the STFT to the obtained frequency bands of interest.

To apply the wavelets to our signal, we proceed in a similar way to reference [60]. First, by means of the DWT and the Daubechies family we decompose the signal into 8 levels (see Figure 9a), in such a way that, at level d7 the frequency range is from 0 to 78 Hz and this is where the frequency components could be found associated with the types of failures mentioned so far. However, observing the d7 level in Figure 9a, it is not enough to make a diagnosis, and in these cases, it is necessary to apply another type of analysis or use other methodologies, as described in reference [101]. Later, CWT with a scale of 1:100, it is applied and whose 2D graph is shown in Figure 9b. Here, in addition to the periodicity of the signal, it can also be seen how as the scale factor increases towards the last low-pass filters, the wavelets compress more and the number of low-frequency components associated with faulty bars or eccentricity becomes more evident. The 3D graph is included in Figure 9c, displaying the periodicity and uniformity or composition of the signal as a function of time. In this last graph, the peaks of the signal occur in the last scales; therefore, by calculating in MATLAB the frequency equivalent of scale 100, the value of 6 Hz is obtained, which is consistent with the results of other signaling techniques.

According to reference [102], one of the disadvantages of classic SA using the FFT is the loss of information when the signal is segmented. This can be compensated by the weighting of the windows. However, this incurs a decrease in spectral resolution. As described in references [45,65], despite the benefits of analysis in the time-frequency domain, since the components associated with the faults may be very close to the fundamental frequency, their identification is complicated, so it is also necessary to determine the frequency at which the analysis should be performed. At high frequencies, a good resolution is obtained in the time domain, while at low frequencies, the resolution is better in the frequency domain.
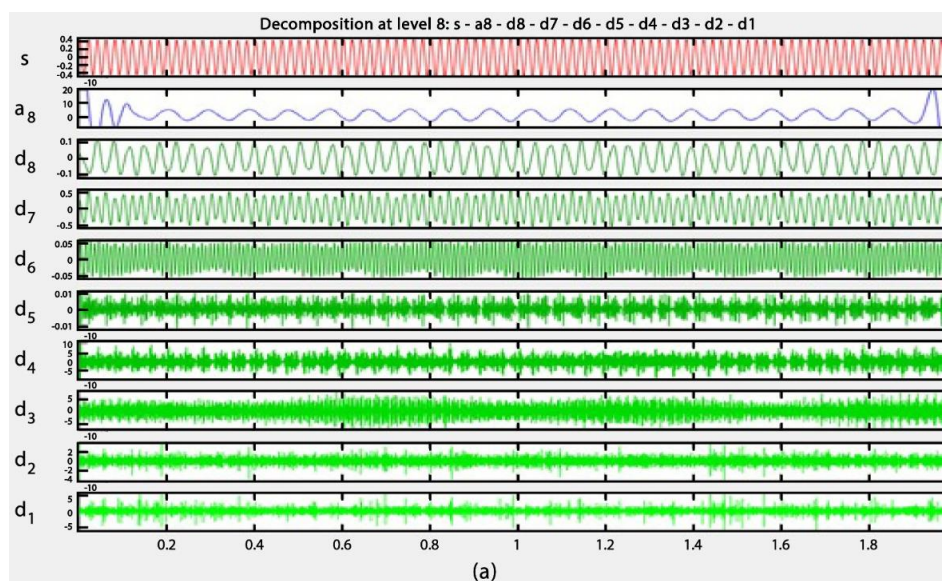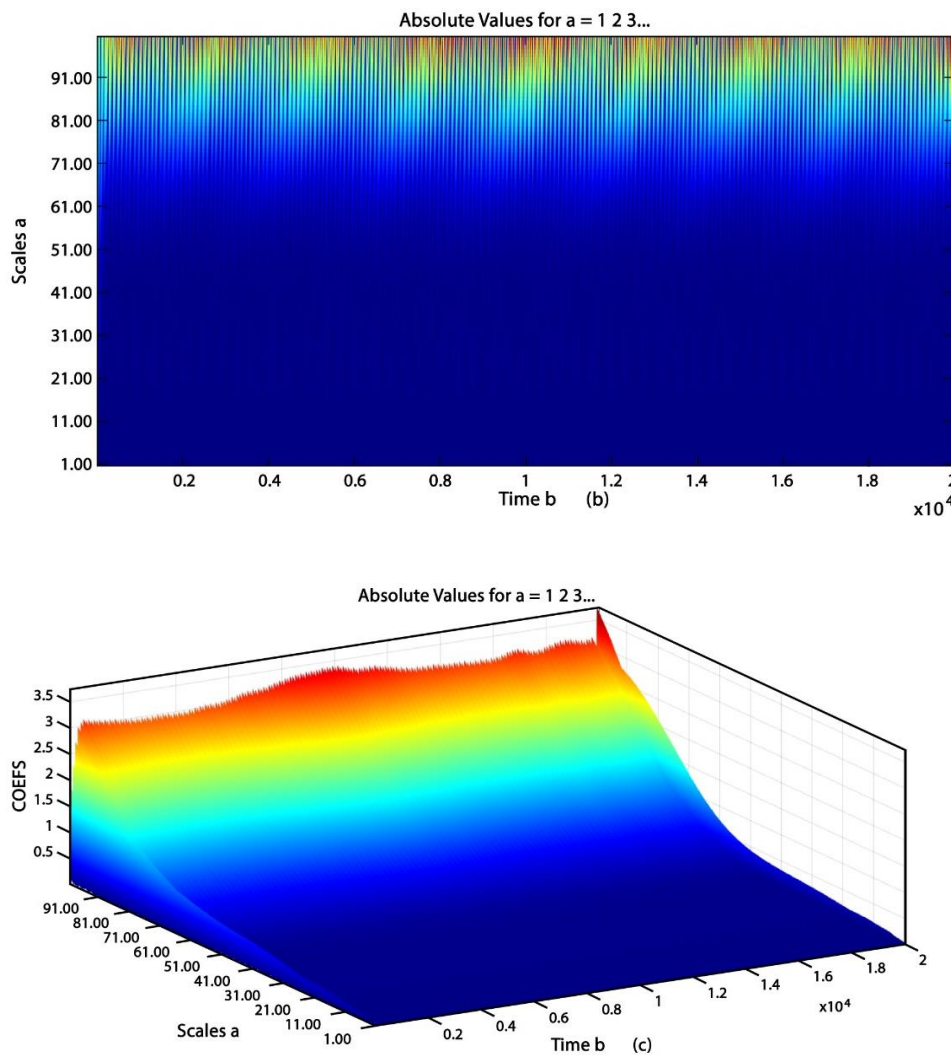

Figure 9. *Cont.*

Figure 9. Application of the wavelet transform to the SCIG signal. (**a**) Decomposition of the current signal using the DWT, (**b**) 2-dimensional continuous wavelet transform, (**c**) 3-dimensional continuous wavelet transform.

According to reference [99], the wavelet transform has the disadvantage of overlap between the frequency bands in which the signal has been separated and the need for an optimal selection of the mother wavelet. To overcome these drawbacks, that report proposes to carry out the analysis by applying both the HT and the wavelet transform to the current signal during startup. According to the authors, based on the experimental studies and in contrast to the classic Fourier analysis, the DWT-based approaches are simple and allow clear and reliable patterns to be obtained. The Hilbert–Huang transform (HHT) has the advantage of avoiding dyadic decomposition, allowing greater security in the study of high-frequency components located on the right-hand side, and IMFs allow a more secure theoretical representation of the waveform composed of the left sidebands on the supply frequency, which cannot be achieved with the DWT. Among the disadvantages are the introduction of signal overlap problems, although this effect is negligible during startup. The patterns obtained are not as clear as in other methods and are more difficult to interpret. There is no a priori relationship between IMFs and frequency bands, making it difficult to select the appropriate number of IMFs to consider for the detection of lateral components. As discussed in reference [99], these conclusions have to be verified in field studies so that the results can be generalized for different operating conditions.

Finally, by applying the Park transform to the generator signal, Figure 10 is obtained. According to reference [97], regardless of the slip, the short circuits between turns or broken bars produce

an alteration in the envelope repeats cyclically to the same supply frequency, causing the elliptical shape of the Park transform graph. Additionally, the comparison of Figure 10 with the results obtained in reference [103] for the diagnosis of broken bars verifies substantial similarity.
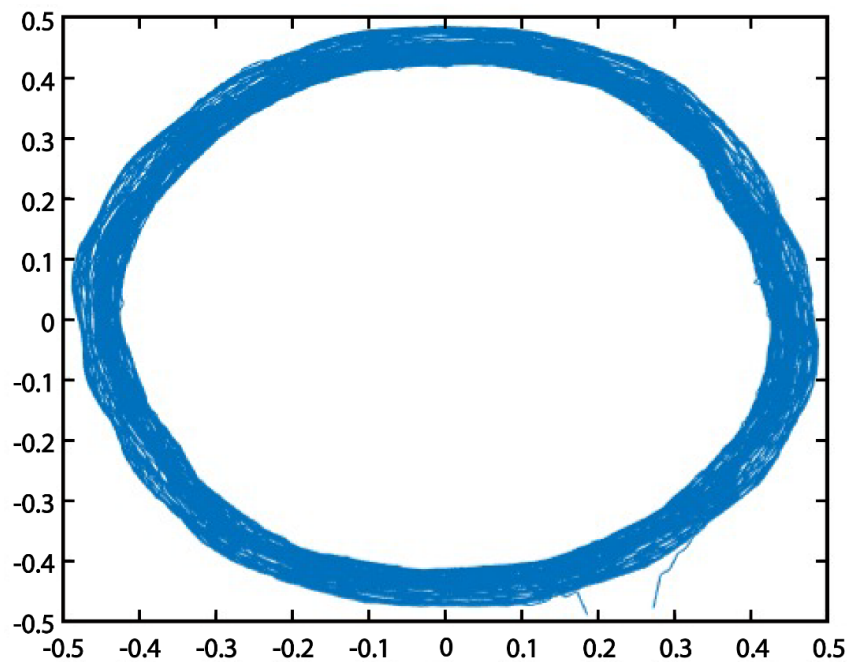

Figure 10. Park vectors of the current signal.

6. Conclusions and Recommendations

Through this research, it has been possible to demonstrate the feasibility of detecting and diagnosing faults in a WT generator using SA of the current signal. According to the models described in the theoretical part of this research, there is at least one indication of failure due to broken bars in the generator under study. The analysis was carried out using various signal processing techniques, obtaining similar results with all techniques. However, the magnitude of the failure has not been included in this investigation. To check the results obtained and to carry out a more in-depth investigation, a periodic sampling could be done to analyze the evolution of the spectrum of the generator current signal.

Although the diagnosis was obtainable with all the signal processing and analysis techniques used, there are some differences. The FT indicates which frequencies exist in the spectrum of a signal, but it does not provide the time at which these frequencies occur, nor does it provide the modulation of the phase. Aliasing and leakage problems can also occur, and in general, this technique is not recommended for transient states. The STFT allows information to be obtained in both the time domain and the frequency domain. However, since it uses a fixed observation window for all frequencies, it cannot adapt to rapid signal changes and cannot eliminate noise. In contrast, the DWT cannot analyze the evolution over time of the frequency composition of each frequency group. The power spectrum does not provide phase information, and the autocorrelation sequence does not provide evidence of nonlinearity. Furthermore, since the power spectrum variance does not tend to zero as the number of samples increases, the second-order periodogram or moment is not a consistent estimator, and it is necessary to resort to third-order estimators such as the bispectrum, MUSIC, and root MUSIC.

Signal processing techniques are a very powerful tool. However, in many cases, especially when conditions are not ideal, the use of these methodologies in isolation is not sufficient, and it is necessary to use other, complementary models to increase the effectiveness of diagnosis. The use of the current signal for the detection and diagnosis of faults in WTs is an area still to be explored, especially through field work. However, based on the few existing references on field studies carried out with WTs in

operation, it can be said in general that when the current signal is used, the diagnostic process is based on the models analyzed in Sections 2 and 3 of this investigation.

According to what was seen in the introduction, in this research we have concentrated on the SCIG. However, the most widely used electric generator in the wind industry is the double feed induction generator (DFIG) which has many characteristics in common with the SCIG. However, since the DFIG has a wound rotor that is feed independently, it has an electrical signal from the stator and another signal from the rotor, which could be studied independently or in combination to detect both rotor and stator faults. Another important aspect to consider is that WTs with DFIG use a power converter to control the rotor current, which modifies the spectrum of the signals and increases the difficulty of diagnosis. To limit the research, we have preferred not to delve into the differences that we would have with the DFIG, since it would be preferable to do another specific field study on this type of generator.

Several of the models seen so far require knowledge of the rotor mechanical speed and/or slip and generator design parameters, among other variables, which are generally not available. Additionally, when signal processing and analysis techniques are used, it is necessary to perform the study for each phase and for each record at the same time, so, considering the three phases of each generator and the total WTs of a WF, the work is very complicated and can lead to diagnostic errors. Besides, almost all the reports used as references rely on a signal that includes an explicitly provoked failure, which was not possible to obtain for this investigation. Despite these aspects, a very useful technique at present is to combine signal processing techniques with artificial intelligence models.

Nomenclature

A_T	torque amplitude
A_{sMi}, A_{sTi}	amplitude of magnetization and torque components
a	$1(120°) = 1e^{j\frac{2\pi}{3}} = -0.5 + j0.866$
a^2	$1(240°) = 1e^{j\frac{4\pi}{3}} = -0.5 - j0.866$
$\overrightarrow{B}$	flux density
$e(n)$	sampled noise
$f_r(\text{Hz})$	rotor frequency
f_{mr}	rotor mechanical frequency
f_{te}	gear frequency
f_v	vibration frequency of bearing failure
$g\,(\theta_r, \theta_{sr})$	air gap function (g in the case of a uniform air gap)
g_o	constant air gap length
$g(t)$	mean air gap length as a function of time
I_L	line current
i_0	average or constant component of the current
i_{sM}, i_{sT}	magnetization and torque components of the stator current
i_{sM0}, i_{sT0}	constant value of magnetization and torque components
J	inertia
k_m	failure modulation index
k_{wh}	winding factor for harmonic h

k_0	$0, 1, 2, 3, 4, 5, \ldots$
k_1	$1,\ 3,\ 5,\ 7,\ 9,\ \ldots$
k_2	$1,\ 2,\ 3,\ \ldots,\ (2p-1)$
k_3	$0, \pm 2,\ \pm 6,\ \pm 10,\ \ldots$
N	number of turns per coil
N_r	number of turns of the rotor winding
n_d	0 for static eccentricity, $1, 2, 3, 4, 5, \ldots$ for dynamic eccentricity
MMF	magnetomotive force
P_i	input power
p	pole pairs
p_d	bearing diameter
P_{Fe}	iron losses
Q_r	rotor slots
R_r	rotor resistance
R_s	stator resistance
S	arbitrary contour surface
s_i	number of complex sinusoids
s	slip per unit
T_0	constant torque component
T_{em}	electromechanical torque
T_T	total torque
T_d	damping torque due to failure
T_{osc}	blade torque under normal conditions
θ_s	angular displacement with reference to the stator
θ_r	rotor angular displacement, rotor surface
θ_{sr}	angular displacement between rotor and stator reference position
φ	phase angle, load or power factor
φ_s	phase shift between the stator and rotor MMFs
φ_d	phase angle of the fault
ω	angular velocity of the feed current
ω_{ro}	constant component of the angular speed of the rotor
ω_s	stator field angular velocity
ω_{mr}	rotor mechanical speed
ω_r	rotor magnetic field speed
ω_f	angular velocity of the fault
Λ^2	Laplace operator
ξ	temporal variable
σ^2	variance
δ_d	dynamic eccentricity index

References

1. Qiao, W.; Lu, D. A Survey on Wind Turbine Condition Monitoring and Fault Diagnosis—Part I: Components and Subsystems. *IEEE Trans. Ind. Electron.* **2015**, *62*, 6536–6545. [CrossRef]
2. Qiao, W.; Lu, D. A Survey on Wind Turbine Condition Monitoring and Fault Diagnosis—Part II: Signals and Signal Processing Methods. *IEEE Trans. Ind. Electron.* **2015**, *62*, 6546–6557. [CrossRef]
3. García Márquez, F.P.; Tobias, A.M.; Pinar Pérez, J.M.; Papaelias, M. Condition monitoring of wind turbines: Techniques and methods. *Renew. Energy* **2012**, *46*, 169–178. [CrossRef]
4. Merizalde, Y.; Hernández-Callejo, L.; Duque-Pérez, O.; Alonso-Gómez, V. Diagnosis of wind turbine faults using generator current signature analysis: A review. *J. Qual. Maint. Eng.* **2019**. [CrossRef]
5. Jin, X.; Cheng, F.; Peng, Y.; Qiao, W.; Qu, L. A comparative study on Vibration- and current-based approaches for drivetrain gearbox fault diagnosis. In Proceedings of the IEEE Industry Applications Society Annual Meeting IAS 2016, Portland, OR, USA, 2–6 October 2016; pp. 1–8. [CrossRef]

6. Henao, H.; Capolino, G.A.; Cabanas, M.N.; Filippetti, F.; Bruzzese, C.; Strangas, E.; Pusca, R.; Estima, J.; Riera-Guasp, M.; Hedayati-Kia, S. Trends in Fault Diagnosis for Electrical Machines: A Review of Diagnostic Techniques. *IEEE Ind. Electron.* **2014**, *8*, 31–42. [CrossRef]

7. Pires Leite, G.; Araújo, A.M.; Carvalho, P.A. Prognostic techniques applied to maintenance of wind turbines: A concise and specific review. *Renew. Sustain. Energy Rev.* **2018**, *81*, 1917–1925. [CrossRef]

8. Seera, M.; Peng Lim, C.; Nahavandi, S.; Kiong Loo, C. Condition monitoring of induction motors: A review and an application of an ensemble of hybrid intelligent models. *Expert Syst. Appl.* **2014**, *41*, 4891–4903. [CrossRef]

9. El Bouchikhi, E.H.; Choqueuse, V.; Benbouzid, M. Induction machine faults detection using stator current parametric spectral estimation. *Mech. Syst. Signal Process.* **2015**, *52–53*, 447–464. [CrossRef]

10. AETS Sudamérica. Estudio de Mercado de Motores Eléctricos en Chile. Santiago de Chile. 2010. Available online: http://dataset.cne. cl/Energia_Abierta/Estudios/Minerg/10.Estudio%20Motores%20El%C3%A9ctricos%20en%20Chile_Final%20(1045).pdf (accessed on 8 October 2019).

11. Stroker, J.J. What's the real cost of higher efficiency? *IEEE Ind. Appl. Mag.* **2003**, *9*, 32–37. [CrossRef]

12. Stavrakakis, G.S. Electrical parts of wind turbines. *Compr. Renew. Energy* **2012**, *2*, 269–328. [CrossRef]

13. Chen, S. Induction Machine Broken Rotor Bar Diagnostics Using Prony Analysis. Master's Thesis, University of Adelaide, Adelaide, Australia, 2008.

14. Pyrhönen, J.; Jokinen, T.; Hrabovcová, V. *Design of Rotating Electrical Machines*; John Wiley & Sons: Chichester, UK, 2008.

15. Bose, B.K. *Modern Power Electronics and AC Drives*; Prentice Hall PTR: Upper Saddle River, NJ, USA, 2002.

16. Yacamini, R.; Smith, K.S.; Ran, L. Monitoring Torsional Vibrations of Electro-mechanical Systems Using Stator Currents. *J. Vib. Acoust.* **1998**, *120*, 72–79. [CrossRef]

17. Toliyat, H.A.; Campbell, S.G. *DSP-Based Electromechanical Motion Control*; CRC PRESS: Boca Raton, FL, USA, 2003.

18. Orille, A.L.; Sowilam, G.M.A.; Valencia, J.A. New simulation of symmetrical three phase induction motor under transformations of park. *Comput. Ind. Eng.* **1999**, *37*, 359–362. [CrossRef]

19. Bonnett, A.H. Root cause AC motor failure analysis with a focus on shaft failures. *IEEE Trans. Ind. Appl.* **2000**, *36*, 1435–1448. [CrossRef]

20. Kia, S.; Henao, H.; Capolino, G. Diagnosis of broken-bar fault in induction machines using discrete wavelet transform without slip estimation. *IEEE Trans. Ind. Appl.* **2009**, *45*, 1395–1404. [CrossRef]

21. Mohanty, A.R.; Kar, C. Fault detection in a multistage gearbox by demodulation of motor current waveform. *IEEE Trans. Ind. Electron.* **2006**, *53*, 1285–1297. [CrossRef]

22. Penman, J.; Seddling, H.G.; Fink, W.T. Detection and Location of Interturn Short Circuits in the Stator Windings of Operating Motors. *IEEE Trans. Energy Convers.* **1994**, *9*, 652–658. [CrossRef]

23. Filippetti, F.; Franceschini, G.; Tassoni, C.; Vas, P. Recent developments of induction motor drives fault diagnosis using AI techniques. *IEEE Trans. Ind. Electron.* **2000**, *47*, 994–1004. [CrossRef]

24. Jung, J.H.; Lee, J.J.; Kwon, B.H. Online diagnosis of induction motors using MCSA. *IEEE Trans. Ind. Electron.* **2006**, *53*, 1842–1852. [CrossRef]

25. Joksimovic, G.M.; Penman, J. The detection of inter-turn short circuits in the stator windings of operating motors. *IEEE Trans. Ind. Electron.* **2000**, *47*, 1078–1084. [CrossRef]

26. Benbouzid, M.E.H. A review of induction motors signature analysis as a medium for faults detection. *IEEE Trans. Ind. Electron.* **2000**, *47*. [CrossRef]

27. Thomson, W.T.; Fenger, M. Current signature analysis to detect induction motor faults. *IEEE Ind. Appl. Mag.* **2001**, *7*, 26–34. [CrossRef]

28. Drozdowski, P.; Duda, A. Influence of magnetic saturation effects on the fault detection of induction motors. *Arch. Electr. Eng.* **2014**, *63*, 489–506. [CrossRef]

29. Bellini, A.; Filippetti, F.; Tassoni, C.; Capolino, G. Advances in diagnostic techniques for induction machines. *IEEE Trans. Ind. Electron.* **2008**, *5*, 4109–4126. [CrossRef]

30. Tavner, P.J. Review of condition monitoring of rotating electrical machines. *IET Electr. Power Appl.* **2008**, *2*, 215–247. [CrossRef]

31. Vas, P. *Parameter Estimation, Condition Monitoring, and Diagnosis of Electrical Machines*; Clarendon Press: New York, NY, USA, 1993.

32. Cameron, J.R.; Thomson, W.T.; Dow, A.B. Vibration and current monitoring for detecting airgap eccentricity in large induction motors. *IEE Proc. B Electr. Power Appl.* **1986**, *133*, 155–163. [CrossRef]

33. Nandi, S.; Toliyat, H.A. Detection of rotor slot and other eccentricity related harmonics in a three phase induction motor with different rotor cages. *IEEE Trans. Energy Convers.* **2001**, *16*, 253–260. [CrossRef]

34. Blödt, M.; Regnier, J.; Faucher, J. Distinguishing load torque oscillations and eccentricity faults in induction motors using stator current wigner distributions. *IEEE Trans. Ind. Appl.* **2009**, *45*, 1991–2000. [CrossRef]

35. Teng, W.; Zhang, X.; Liu, Y.; Kusiak, A.; Ma, Z. Prognosis of the remaining useful life of bearings in a wind turbine gearbox. *Energies* **2017**, *10*, 32. [CrossRef]

36. Lee, Y.; Cheatham, T.; Wiesner, J. Application of Correlation Analysis to the Detection of Periodic Signals in Noise. *IEEE Trans. Ind Electron. Proc. IRE* **1950**, *38*, 1165–1171. [CrossRef]

37. Dalpiaz, G.; Rivola, A.; Rubini, R. Effectiveness and sensitivity of vibration processing techniques for local fault detection in gears. *Mech. Syst. Signal Process.* **2000**, *14*, 387–412. [CrossRef]

38. Jardine, A.; Lin, D.; Banjevic, D. A review on machinery diagnostics and prognostics implementing condition-based maintenance. *Mech. Syst. Signal Process.* **2006**, *20*, 1483–1510. [CrossRef]

39. Poyhonen, S.; Jover, P.; Hyotyniemi, H. Signal processing of vibrations for condition monitoring of an induction motor. In Proceedings of the First International Symposium on Control, Communications and Signal Processing, New York, NY, USA, 21–24 March 2004. [CrossRef]

40. Baillie, D.; Mathew, J. A comparison of autoregressive modeling techniques for fault diagnosis of rolling element bearings. *Mech. Syst. Signal Process.* **1996**, *10*, 1–17. [CrossRef]

41. Zhan, Y.; Makis, V.; Jardine, A. Adaptive model for vibration monitoring of rotating machinery subject to random deterioration. *J. Qual. Maint. Eng.* **2003**, *9*, 351–375. [CrossRef]

42. Attoui, I.; Omeiri, A. Fault Diagnosis of an Induction Generator in a Wind Energy Conversion System Using Signal Processing Techniques. *Electr. Power Compon. Syst.* **2015**, *43*, 2262–2275. [CrossRef]

43. Pinto, M. Procesamiento de Señales Utilizando el Análisis Tiempo-Frecuencia. Master's Thesis, Centro de Investigación y Tecnología Digital, Instituto Politécnico Nacional, Tijuana, Mexico, 2005.

44. Serie Discreta de Fourier. Available online: http://www.ehu.eus/Procesadodesenales/tema3/71.html (accessed on 27 December 2019).

45. Artigao, E.; Honrubia-Escribano, A.; Gomez-Lazaro, E. Current signature analysis to monitor DFIG wind turbine generators: A case study. *Renew. Energy* **2018**, *116*, 5–14. [CrossRef]

46. Pons-Llinares, J.; Antonino-Daviu, J.; Riera-Guasp, M.; Lee, S.; Kang, T.; Yang, C. Advanced Induction Motor Rotor Fault Diagnosis Via Continuous and Discrete Time–Frequency Tools. *IEEE Trans. Ind. Electron.* **2015**, *63*, 1791–1801. [CrossRef]

47. Scarpazza, D. A Brief Introduction to the Wigner Distribution. 2003. Available online: http://www.scarpaz.com/Attic/Documents/TheWignerDistribution.pdf (accessed on 24 April 2020).

48. Misiti, M.; Misiti, Y.; Oppenheim, G.; Poggi, J. *Wavelet Toolbox for Use with Matlab*; The Math Works Inc.: Natick, MA, USA, 2004. Available online: https://www.ltu.se/cms_fs/1.51590!/wavelet%20toolbox%204%20user\T1\textquoterights%20guide%20(larger%20selection).pdf (accessed on 29 January 2019).

49. Cooley, J.; Tukey, J. An algorithm for the machine calculation of complex Fourier series. *Math. Comput.* **1965**, *19*, 297–301. [CrossRef]

50. Rabiner, L.; Schafer, R. Introduction to Digital Speech Processing. *Found. Trends Signal Process.* **2007**, *1*, 1–194. [CrossRef]

51. Cohen, L. Time-Frequency Distributions: A Review. *Proc. IEEE* **1989**, *77*, 941–981. [CrossRef]

52. Amirat, Y.; Choqueuse, V.; Benbouzid, M. Condition monitoring of wind turbines based on amplitude demodulation. In Proceedings of the IEEE International Energy Conference, Manama, Bahrain, 18–22 December 2008. [CrossRef]

53. Harris, C.; Piersol, A. *Shock and Vibration Handbook*, 5th ed.; McGraw Hill: New York, NY, USA, 2002; ISBN 0-07-137081-1.

54. Shi, L.; Qiu, J.; Xu, G.; Yang, J.; Wang, J. Online detection for blade imbalance of doubly fed induction generator wind turbines based on stator current. In Proceedings of the 2nd International Conference on Power and Renewable Energy (ICPRE), Chengdu, China, 20–23 September 2017. [CrossRef]

55. Jin, X.; Cheng, F.; Peng, Y.; Qiao, W.; Qu, L. Drivetrain Gearbox Fault Diagnosis: Vibration and Current Based Approaches. *IEEE Ind. Appl. Mag.* **2018**, *24*, 56–66. [CrossRef]

56. Cheng, F.; Qu, L.; Qiao, W.; Wei, C.; Hao, L. Fault Diagnosis of Wind Turbine Gearboxes Based on DFIG Stator Current Envelope Analysis. *IEEE Trans. Sustain. Energy* **2010**, *10*, 1044–1053. [CrossRef]

57. Ibrahim, R.; Watson, S.; Djurović, S.; Crabtree, C. An Effective Approach for Rotor ElectricalAsymmetry Detection in Wind Turbine DFIGs. *IEEE Trans. Ind. Electron.* **2018**, *65*, 8872–8881. [CrossRef]

58. Mallat, S. A theory for multiresolution signal decomposition: The wavelet representation. *IEEE Trans. Pattern Anal. Mach. Intell.* **1989**, *11*, 674–693. [CrossRef]

59. Gueye-Lo, N.; Soualhi1, N.; Frini1, M.; Razik, H. Gear and Bearings Fault Detection Using Motor Current Signature Analysis. In Proceedings of the IEEE Conference on Industrial Electronics and Applications, Wuhan, China, 31 May–2 June 2018. [CrossRef]

60. Kar, C.; Mohanty, A.R. Monitoring gear vibrations through motor current signature analysis and wavelet transform. *Mech. Syst. Signal Process.* **2006**, *20*, 158–187. [CrossRef]

61. Gong, X.; Qiao, W.; Zhou, W. Incipient bearing fault detection via wind generator stator current and wavelet filter. In Proceedings of the 36th Annual Conference on IEEE Industrial Electronics Society IECON, Glendale, AZ, USA, 7–10 November 2010; pp. 2615–2620. [CrossRef]

62. Ordaz-Moreno, A.; Romero-Troncoso, R.; Vite-Frías, J.; Rivera-Gillen, J.; Garcia-Perez, A. Automatic Online Diagnosis Algorithm for Broken-Bar Detection on Induction Motors Based on Discrete Wavelet Transform for FPGA Implementation. *IEEE Trans. Ind. Electron.* **2008**, *55*, 2193–2202. [CrossRef]

63. Antonino-Daviu, J.; Riera-Guasp, M.; Roger-Folch, J.; Molina, M. Validation of a new method for the diagnosis of rotor bar failures via wavelet transformation in industrial induction machines. *IEEE Trans. Ind. Appl.* **2006**, *42*, 990–996. [CrossRef]

64. Antonino-Daviu, J.; Jover, P.; Riera-Guasp, M.; Roger-Folch, J.; Arkkio, A. DWT analysis of numerical and experimental data for the diagnosis of dynamic eccentricities in induction motors. *Mechan. Syst. Signal Process.* **2007**, *21*, 2575–2589. [CrossRef]

65. Kia, S.H.; Henao, H.; Capolino, G.A. Torsional vibration effects on induction machine current and torque signatures in gearbox-based electromechanical system. *IEEE Trans. Ind. Electron.* **2009**, *56*, 4689–4699. [CrossRef]

66. Shinde, S.; Gadre, V. An uncertainty principle for real signals in the fractional Fourier transform domain. *IEEE Xplore* **2001**, *49*, 2545–2548. [CrossRef]

67. Swami, A. HOSA-Higher Order Spectral Analysis Toolbox. Available online: https://www.mathworks.com/matlabcentral/fileexchange/3013-hosa-higher-order-spectral-analysis-toolbox (accessed on 24 March 2020).

68. Goshvarpour, A.; Goshvarpour, A.; Rahati, S.; Saadatian, V. Bispectrum estimation of electroencephalogram signals during meditation. *Iran. J. Psychiatry Behav. Sci.* **2012**, *6*, 48–54.

69. Chow, T.; Fei, G. Three phase induction machines asymmetrical faults identification using bispectrum. *IEEE Trans. Energy Convers.* **1995**, *10*, 688–693. [CrossRef]

70. Ning, T.; Bronzino, J.D. Autoregressive and Bispectral Analysis Techniques: EEG Applications. *IEEE Eng. Med. Biol. Mag.* **1990**, *9*, 47–50. [CrossRef] [PubMed]

71. Nikias, C.L.; Raghuveer, M.R. Bispectrum Estimation: A Digital Signal Processing Framework. *Proc. IEEE* **1987**, *75*, 869–891. [CrossRef]

72. Gu, F.; Shao, Y.; Hu, N. Electrical motor current signal analysis using a modified bispectrum for fault diagnosis of downstream mechanical equipment. *Mech. Syst. Signal Process.* **2011**, *25*, 360–372. [CrossRef]

73. Saidi, L.; Fnaiech, F.; Henao, H. Diagnosis of broken-bars fault in induction machines using higher order spectral analysis. *ISA Trans.* **2013**, *52*, 140–148. [CrossRef]

74. Gu, F.; Wang, T.; Alwodai, A. A new method of accurate broken rotor bar diagnosis based on modulation signal bispectrum analysis of motor current signals. *Mech. Syst. Signal Process.* **2015**, *50–51*, 400–413. [CrossRef]

75. Li, D.Z.; Wang, W.; Ismail, F. An Enhanced Bispectrum Technique with Auxiliary Frequency Injection for Induction Motor Health Condition Monitoring. *IEEE Trans. Instrum. Meas.* **2015**, *64*, 2679–2687. [CrossRef]

76. Garcia-Perez, A.; Romero-Troncoso, R.D.J.; Cabal-Yepez, E.; Osornio-Rios, R.A. The application of high-resolution spectral analysis for identifying multiple combined faults in induction motors. *IEEE Trans. Ind. Electron.* **2012**, *58*, 2002–2010. [CrossRef]

77. Cupertino, F.; de Vanna, E.; Salvatore, L.; Stasi, S. Analysis techniques for detection of IM broken rotor bars after supply disconnection. *IEEE Trans. Ind. Appl.* **2004**, *40*, 526–533. [CrossRef]

78. Kia, S.H.; Henao, H.; Capolino, G.A. A high-resolution frequency estimation method for three-phase induction machine fault detection. *IEEE Trans. Ind. Electron.* **2007**, *54*, 2305–2314. [CrossRef]

79. Chakkor, S.; Baghouri, M.; Hajraoui, A. ESPRIT method enhancement for real-time wind turbine fault recognition. *Int. J. Power Electron. Drive Syst. Porto* **2015**, *5*, 4. [CrossRef]

80. Lobos, T.; Rezmer, J.; Koglin, H. Analysis of Power System Transients using Wavelets and Prony Method. In Proceedings of the IEEE Power Tech Conference, Porto, Portugal, 10–13 September 2001. [CrossRef]

81. Janik, P.; Leonowicz, Z.; Rezmer, J. Advanced Signal Processing Methods for Evaluation of Harmonic Distortion Caused by DFIG Wind Generator. *IEEE Trans. Ind. Appl.* **2006**, *42*, 1454–1463.

82. Zidani, F.; Benbouzid, M.; Diallo, D.; Naït-Saïd, M. Induction Motor Stator Faults Diagnosis by a Current Concordia Pattern-Based Fuzzy Decision System. *IEEE Trans. Energy Convers.* **2003**, *18*, 225–2238. [CrossRef]

83. Grainger, J.; Stevenson, W. *Power System Analysis*, 1st ed.; McGraw Hill: New York, NY, USA, 2012; ISBN 007-061293-5.

84. Bacha, K.; Salem, S.; Chaari, A. An improved combination of Hilbert and Park transforms for fault detection and identification in three-phase induction motors. *Int. J. Electr. Power Energy Syst.* **2012**, *43*, 1006–1016. [CrossRef]

85. Sahraoui, M.; Ghoggal, A.; Guedidi, S.; Zouzou, S. Detection of inter-turn short-circuit in induction motors using Park-Hilbert method. *Int. J. Syst. Assur. Eng. Manag.* **2014**, *5*, 337–351. [CrossRef]

86. Cardoso, A.; Saraiva, V. Computer-aided detection of airgap eccentricity in operating three-phase induction motors by Park's vector approach. *IEEE Trans. Ind. Appl.* **1993**, *29*, 897–901. [CrossRef]

87. Cardoso, A.; Cruz, S.; Carvalho, J.; Saraiva, E. Rotor cage fault diagnosis in three phase induction motors, by Park's vector approach. *Electric Mach. Power Syst.* **1995**, *28*, 289–299. [CrossRef]

88. Cherif, B.; Bendiabdellah, A.; Khelif, M. Detection of open-circuit fault in a three-phase voltage inverter fed induction motor. *Int. Rev. Autom. Control* **2016**, *96*, 374–382. [CrossRef]

89. Vilhekar, T.; Ballal, M.; Suryawanshi, H. Application of multiple parks vector approach for detection of multiple faults in induction motors. *J. Power Electron.* **2017**, *17*, 972–982. [CrossRef]

90. Nandi, S.; Toliyat, H.A.; Li, X. Condition monitoring and fault diagnosis of electrical motors—A review. *IEEE Trans. Energy Convers.* **2001**, *20*, 719–729. [CrossRef]

91. Al Ahmar, E.; Choqueuse, V.; Benbouzid, M.E.H.; Amirat, Y.; El Assad, J.; Karam, R.; Farah, S. Advanced signal processing techniques for fault detection and diagnosis in a wind turbine induction generator drive train: A comparative study. In Proceedings of the IEEE Energy Conversion Congress and Exposition ECCE 2010, Atlanta, GA, USA, 12–16 September 2010; pp. 3576–3581. [CrossRef]

92. Taylor, J. *The Vibration Analysis Handbook*, 2nd ed.; Vibration Consultants: Cambridge, MA, USA, 2003; ISBN 9780964051720.

93. Gong, X.; Qiao, W. Imbalance Fault Detection of Direct-Drive Wind Turbines Using Generator Current Signals. *IEEE Trans. Energy Convers.* **2012**, *27*, 468–476. [CrossRef]

94. Zhivomirov, H. On the Development of STFT-analysis and ISTFT-synthesis Routines and their Practical Implementation. *TEM J.* **2019**, *8*, 56–64. [CrossRef]

95. Hafeez, S.; Zaide, C.; Siddiqui, A. Broken rotor bar detection of single phase induction motor using Wigner-Ville Distributions. In Proceedings of the IEEE 18th Conference on Emerging Technologies & Factory Automation, Cagliari, Italy, 10–13 September 2013. [CrossRef]

96. Randall, R.; Antoni, J. Rolling element bearing diagnostics—A tutorial. *Mech. Syst. Signal Process.* **2011**, *25*, 485–520. [CrossRef]

97. Da Silva, A.; Povinelli, R.; Demerdash, N. Induction machine broken bar and stator short-circuit fault diagnostics based on three-phase stator current envelopes. *IEEE Trans. Ind. Electron.* **2008**, *55*, 1310–1318. [CrossRef]

98. Jaksch, I. Faults diagnosis of three-phase induction motors using envelope analysis. In Proceedings of the 4th IEEE International Symposium on Diagnostics for Electric Machines, Power Electronics and Drives, SDEMPED 2003, Atlanta, GA, USA, 24–26 August 2003; pp. 289–293. [CrossRef]

99. Antonino-Daviu, J.A.; Riera-Guasp, M.; Roger-Folch, J.; Perez, R.B. An Analytical Comparison between DWT and Hilbert-Huang-Based Methods for the Diagnosis of Rotor Asymmetries in Induction Machines. In Proceedings of the IEEE Industry Applications Annual Meeting, New Orleans, LA, USA, 23–27 September 2007; pp. 1932–1939. [CrossRef]

100. Blödt, M.; Chabert, M.; Regnier, J.; Faucher, J. Mechanical load fault detection in induction motors by stator current time-frequency analysis. *IEEE Trans. Ind. Appl.* **2006**, *42*, 1454–1463. [CrossRef]

101. Riera-Guasp, M.; Antonino-Daviu, J.A.; Pineda-Sanchez, M.; Puche-Panadero, R.; Perez-Cruz, J. A general approach for the transient detection of slip-dependent fault components based on the discrete wavelet transform. *IEEE Trans. Ind. Electron.* **2008**, *55*, 4167–4180. [CrossRef]

102. Benbouzid, M.E.H.; Vieira, M.; Theys, C. Induction motors faults detection and localization using stator current advanced signal processing techniques. *IEEE Trans. Power Electron.* **1999**, *14*, 14–22. [CrossRef]

103. Szabo, L.; Erno, K. An Overview on Induction Machine's Diagnosis Methods. 2008. Available online: https://www.researchgate.net/publication/38112249_An_Overview_on_Induction_Machine\T1\textquoterights_Diagnosis_Methods (accessed on 24 April 2020).

Publisher's Note: MDPI stays neutral with regard to jurisdictional claims in published maps and institutional affiliations.